THE STUDY OF AEROSOL MICROPHYSICAL AND OPTICAL PARAMETERS, TOTAL COLUMNAR OZONE AND WATER VAPOR CONTENT DERIVED FROM SUNPHOTOMETER

By

Anteneh Getachew

SUBMITTED IN PARTIAL FULFILLMENT OF THE
REQUIREMENTS FOR THE DEGREE OF
MASTER OF SCIENCE IN PHYSICS
AT
ADDIS ABABA UNIVERSITY
ADDIS ABABA, ETHIOPIA
JULY 2009

ADDIS ABABA UNIVERSITY

DEPARTMENT OF

PHYSICS

Supervisor: Dr. Gizaw Mengistu

Examiners: Dr. Feleke Zewge

Prof. Solomon Billign

ADDIS ABABA UNIVERSITY

Date: **July 2009**

Author: **Anteneh Getachew**

Title: **The Study of aerosol microphysical and Optical parameters, Total columnar Ozone and water vapor content derived from sunphotometer**

Department: **Physics**

Degree: **M.Sc.** Convocation: **June** Year: **2009**

Permission is herewith granted to Addis Ababa University to circulate and to have copied for non-commercial purposes, at its discretion, the above title upon the request of individuals or institutions.

Signature of Author

Table of Contents

List of Figures

Abstract

The spectral aerosol optical depth measurements are estimated over Addis Ababa (09.033N , 38.7E) at 2445m a.m.s.l. from the measurements of direct solar irradiance at different wavelengthes in the range between 305.3-1020nm using a hand held 5-channel Microtops II sunphotometer (Solar light co. USA) for the first time. Results show wavelength dependence of aerosol optical depth (AOD) which gradually decreases with increasing wavelength, having mean value of 0.209 ($\pm$0.0625) at 1020 nm optical channel. The $\mathring{A}$ngstrom exponent α and turbidity β were found to be inversely related with a good anticorrelation ($R = -0.807$) and the $\mathring{A}$ngstrom exponent α was observed to be small in the range from (0.204) to (0.993) with a mean value of (0.627) indicates the presence of coarse mode particles over the site. Temporal variation of both AOD and retrieved columnar size distribution (ASD) show minimum value during the noon time. Large value with large variability in AOD and ASD are observed in April, 2009 as compered to March and May, 2009. This is attributed to the long range transported aerosols from different source. A good positive correlation between aerosol optical depth (AOD) and precipitable water content (PWC) were observed during the measurements of March and may which attributed to the presence of hygroscopic aerosols over the site. The day-to-day variations in total columnar ozone (TCO) were found to be in fair agreement ($10-14\%$) deviation from TOMS satellite data for all the experimental days, having mean observed value of 294.45 ($\pm$6.61) DU over the station.

Keywords: Aerosols; Aerosol optical depth; Aerosol size distribution; $\mathring{A}$ngstrm parameters; total columnar ozone; and precipitable water content.

Acknowledgements

I offer my deepest gratitude first and foremost to my supervisor Dr. Gizaw Mengistu for his unlimited and constructive guidance, advice, suggestions, comments and friendly approach during this research. His tireless follow up and his consistent support will be in my memory forever. I would like to gratitude Dr. Feleke Zewge and Dr. V. Morris for their contractive advice and material support.

My strongest gratitude is addressed to my brother Ato Tesfaye Getachew and his beloved wife Meseret Abebaw for their unlimited support for me and my family. They are the hero of my success. I am also thankful to Selam, brothers, sisters and friends for their patient and support. I have derived materials from many research journals and books, and I am indebted to the authors of those publications and books. At last but not least I would like to thank My Dad.

Introduction

Aerosols play an important role in earth's radiation budget, air quality and environmental health. On a global scale, the natural sources of aerosols are more important than the anthropogenic aerosols, but regionally anthropogenic aerosols are more important . The optical properties of atmospheric aerosol are determined by their chemical composition, concentration, size and internal structure. All these characteristics vary in space and time (i.e. at any time new particles can enter or leave the atmosphere under study) depending on local and reginal events of natural and anthropogenic nature such as bio-mass burning, urban and non-urban processes, volcanic eruptions and airborne soil particles. This causes a difficult task in monitoring the atmospheric aerosols, and thus significant efforts have been made to improve aerosol characterization by using in situ measurements from ground-based remote sensing, satellite observations and aerosol transport. Therefore, a deeper understanding about the processes plays a key role in the tropospheric radiative budget, which is strongly dependant on the aerosol content of the lower troposphere and in air quality problems concerning urban and non-urban processes.

Variations in optical properties of aerosols distribution in the atmosphere are one of the most fundamental geophysical variables for computing the scattering phase function, single scattering albedo and the spectral and air mass variation of aerosol optical depths. Spectral and air mass dependance of aerosol optical depths are important for modelling radiative effects of aerosols in the near-surface atmosphere.

Particulate pollution in the atmosphere can be assessed using various ways like measuring aerosol mass concentration, atmospheric turbidity, counting air born particles etc. The presence of aerosol in the lower atmosphere is usually assumed to attenuate incoming solar radiation by scattering and absorption. The back-scattered fraction of the solar beam increases the earth's albedo and therefore reduces the amount of solar energy available for heating the earth, thereby cooling the earth. Atmospheric heating or cooling depends on the chemical composition of the aerosol, micro-physical and optical properties and spatial distribution of the particles. Optical properties of aerosols can vary greatly depending on environmental conditions as well as on local source. Moreover, these properties depend on the aerosol size distribution as well as on the refractive index and the shape of particles.

Atmospheric aerosol particles may also play an important role in the global radiation balance by modulating the climate system directly by scattering and absorbing solar and terrestrial radiation and, indirectly, by serving as cloud condensation nuclei to influence cloud microphysics and hence cloud radiative properties. The chemical composition and size distribution of the aerosol are important in quantifying these

radiative effects, through influencing absorption and scattering. The size and composition also influence the hygroscopic properties of the aerosol particles and their ability to act as cloud condensation nuclei, and therefore affect cloud formation. Aerosol particles can also participate in heterogeneous reactions in the atmosphere, which are both composition and morphology dependent.

One of the most important optical properties of aerosols used in the radiative transfer calculation is the Aerosol Optical Depth (AOD). It is defined as the attenuation of direct solar radiation passing through the atmosphere by scattering (angular redistribution of energy) and absorption (conversion of energy into either heat or photochemical change) due to aerosols. Monitoring AOD at different wavelengths is useful for deriving additional information on the size distribution of particles, as well as the study of its variation with season, which in turn helps to identify the variation in the source strength of different particles emitted into atmosphere. On the study area measurements of AOD have been done once in past using home made pyrheliometer. The study have considerably in reach our knowledge on AOD over the study area and provide some background information, overcoming the limitations of these measurements, we conducted measurements using a five channel Microtops II. This study revealed several aspects of aerosol extinction features and brought out the need for detailed studies by making measurements for a considerable period of tim.

Apart from atmospheric aerosols, ozone and water vapor content present in the atmosphere are also important atmospheric constituents that play key role in the radiation balance of the Earth-atmosphere system (Ranjan et al.,2007). Changes in

tropospheric ozone are mainly associated with increase in the urban pollution and biomass burning. The column ozone concentration has been measured in the past by two well-known passive ground-based instruments, namely, Dobson and Brewer spectrophotometers. But these instruments are very expensive, heavy and huge. There has been a need for less expansive, more portable and compact instruments that can measure ozone with reasonable accuracy over different environments. In this study, a hand-held, advanced ozone monitor has been used for the first time to measure total column ozone (TCO) and its variability over Addis Ababa.

Atmospheric aerosols and various gases interact in different ways with atmospheric water vapor and thus producing various effects. There have been a number of studies of the change of aerosol properties as a function of water vapor in terms of relative humidity (Hanel, 1972). Distribution of water content in the atmosphere is a good indicator of the dynamics of the circulation systems in the atmosphere (Raj et al., 2004). It is well known that the precipitable water content present in the atmosphere can vary at very short time scales(Ranjan et al.,2007). Therefore, a continuous monitoring of precipitable water content with good temporal resolution is essential for understanding various dynamical processes occurring within the atmosphere. A sunphotometer that has been used in this study, works on the method of differential optical absorption and scattering (DOAS) that allows monitoring the precipitable water content in the atmosphere on a real-time scale with reasonable temporal resolution, which is otherwise difficult to make such measurements with other in-situ instruments.

In this paper, we study the spectral and temporal variation of aerosol optical depth and angstrom parameters and the relation between angstrom parameters (Angstrom exponent α and turbidity coefficient β). We also study the day-to-day variation and association of mean AOD, Angstrom parameters, total columnar ozone and precipitable water vapor, for clear sky days of March, April and May 2009, over the study area using five channel Microtops II. These results will contribute to understanding the regional characteristics of aerosols and in helping with aerosol modelling.

The thesis is organized as follows: In chapter one, we present atmospheric aerosol definitions, aerosols Microphysical and chemical properties, climatic effects of aerosols and particle size distribution. In chapter two, we present the optical properties of aerosols, radiative transfer equation for plane parallel atmosphere, Beer-Bouguer law, Å ngstrom parameters, Mie scattering. In chapter three, we present, retrieval of aerosol size distributions from optical thickness measurements. In chapter four, we present, source of ozone, stratospheric ozone chemistry, distribution and absorption band of ozone. In chapter five, we present, materials used and methodologies for measuring ozone and precipitable water content, determination of aerosol optical depth from the measured signal, determination of atmospheric turbidity and air mass back trajectory analysis using HYSPLIT model. In chapter six, we present the results and discussion. Finally, in chapter seven we present the conclusions.

Chapter 1

Atmospheric Aerosol

1.1 Aerosol Definition and Sources

Atmospheric aerosols are solid or liquid particles (or both) suspended in air with diameters between about $0.002\mu m$ to about $100\mu m$. Interaction of the particulate matter (aerosols and clouds particles) with electromagnetic radiation is controlled by particle size, composition and shape. Atmospheric particles vary greatly depending on sources, production mechanisms, sizes, shapes, chemical composition, amount, distribution in space and time, and how long they survive in the atmosphere (i.e. lifetime).

Primary atmospheric aerosols are particulate that are emitted directly into the atmosphere (for instance, sea-salt, mineral aerosols, volcanic dust, smoke and soot, some organic). Secondary atmospheric aerosols are particulate that are formed in the atmosphere by gas-to-particles conversion processes (for instance, sulphates, nitrates, some organic).

Aerosols can be found in the stratosphere, where they are ejected mainly by strong volcanic eruptions, and in the troposphere. The sources of tropospheric aerosols can be natural (like sea-salt, dust storm, biomass burning, volcanic debris, gas-to-particle conversion) or anthropogenic (like biomass and fossil fuel burning, gas-to-particle conversion, industrial processes, agricultural activities). The main individual chemical species that constitute the tropospheric aerosols are sulphates, soot, sea-salt, various minerals. Generally, the aerosols are a mixture of various components with different mixing ratios.

In spite of high temporal and spatial aerosol variability, there are a rather limited number of general categories of tropospheric aerosol types with distinctly different optical properties. The following four general aerosol types are associated with different sources and emission mechanisms and are expected to exhibit significant differences in optical properties: urbanindustrial aerosol from fossil fuel combustion in populated industrial regions, biomass burning aerosol produced by forest and grassland fires, desert dust blown into the atmosphere by wind, and aerosol of marine origin.

1.2 Microphysical parameters and chemical composition of atmospheric aerosol

For a correct simulation of light propagation in atmosphere, one needs to know the microphysical properties and type of aerosol in the propagation channel. This is rarely known in advance. Therefore, a number of models have been proposed to characterize average microphysical characteristics of aerosol.

The aerosol size distributions are determined by their source, transport and removal conditions. Generally, the mode structure includes three groups of modes, which are characterized by different radii:

- An ultra-fine particle mode, or Aitken mode, or nucleation mode. Small particle formation takes place, particle number rises rapidly up by coagulation and accumulate in the range of the accumulation mode. The range of radii is $0.005 - 0.05\mu m$;
- An accumulation mode, or sub-micron particle mode. Most of the aerosols are in the accumulation mode, where the formation and growth processes slow down and the removal processes are still not effective; therefore this mode is for the long-living aerosol species. The range of radii is $0.05 - 0.5\mu m$;
- A coarse particle mode, or super-micron particle mode. Examples are soil dust, sea salt, small droplets. For these modes the removal processes are more efficient. The range of radii is $0.5 - 10\mu m$.

Beside the size distribution, the optical properties of the aerosol are determined also by their chemical composition. Aerosol types consist of different components, often mixed together. The aerosol components can be mixed externally and/or internally. External mixing is defined by different particles having different composition, while internal mixing is given by single particles containing more than one component. The most important mixing state for the aerosol is the mixing with water, which causes the particles growth with humidity.

Therefore, it is of importance to have a classification of main aerosol types. Then these types can be used as building blocks for the development of microphysical and optical aerosol models. The main aerosol types are discussed below:

Sea-Salt aerosol (SSA) are tiny air born droplets of sea water, or sea salt rich particles formed by the evaporation of water from such droplets. Dried sea salt aerosol are shown in Fig 1.1. Physical processes occurring at the surface of the ocean inject large quantities of aerosol particles into the troposphere the primary pathway of creation is the bursting of air bubbles during whitecap formation and wave breaking, Fig 1.2 shows this process. When bubbles burst a small jet of water forms that can eject up to 15cm above the water surface. Sea-Salt particles cover a wide size range belong to the coarse particle size mode. Sea-Salt aerosols occupy a wide size range from $0.05 - 10\mu m$ diameter, and have correspondingly wide range of atmospheric lifetimes.

The largest droplets fall close to their area of origin. Only the smallest aerosol particles with sizes from approximately 0.1 to $1\mu m$ (e.g., those formed by the bursting of bubbles at the ocean surface) are of a primary importance to the large-scale atmospheric aerosol properties. These particles can exist in the atmosphere for a long time and have been identified over continents as well. The strength of the ocean as a source of salt particles depends on wind speed, sea salt aerosols are optically important at wind speeds above 7 to 10 m/s. This aerosol may be the dominant contributors to both light attenuation and cloud nuclei in those regions of the marine atmosphere where wind speeds are high and/or other aerosol sources are weak. Chemically, these

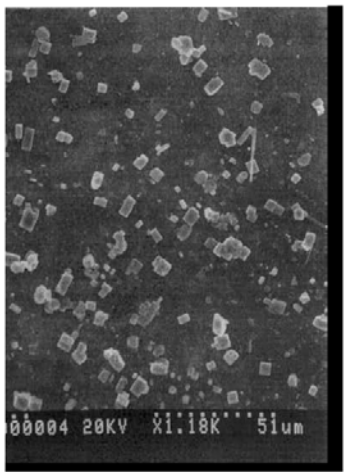

Figure 1.1: Scanning electron photograph of dried sea-salt particles for marine air conditions collected at Mace Head on the west coast of Ireland (Alexander and Kokhanovsky 2008). The width of the picture represents $51\mu m$.

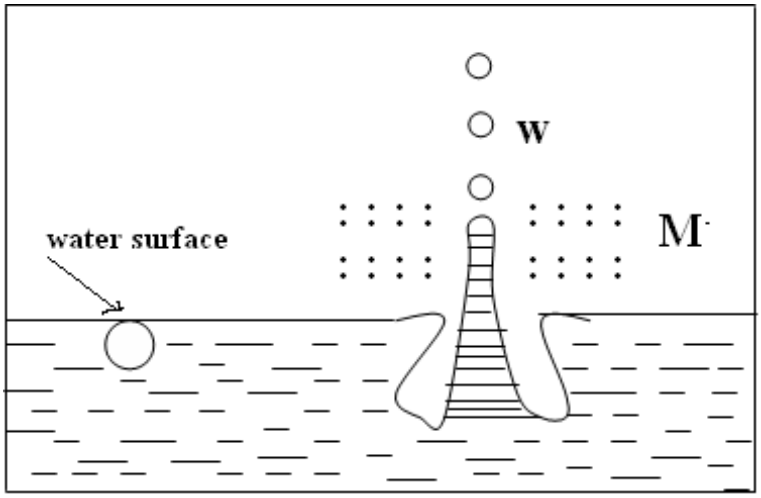

Figure 1.2: Formation of spray droplets during explosion of air bubbles from the surface of water(from trace element),W = droplets, M = Water particles

aerosols are comprised mainly of $NaCl, KCl, CaSO_4, (NH_4)_2SO_4$. They are hygroscopic able to attract water from the air. Thus the size and shape of the particles varies with humidity.

Dust aerosol (DA) originates from the land surface. These mineral aerosols are made up of materials derived from the Earth's crust and are composed of solid particles. Most of them are rich in Silicon, iron, aluminium oxides and calcium carbonate so they are not soluble in water. Therefore, dramatic changes of the aerosol particle shape and structure in the humidity field are rare events as compared to sea-salt aerosols. However, the mineral core can be covered by a water or ice shell in high humidity conditions ($> 75\%$). This will modify the optical properties of these particles. Fig 1.3 shows the scanning electron photograph of dust aerosols. Most of the mineral aerosols in the air come originally from the desert regions, about half of the total mineral aerosols in the air come originally from the Saharan Desert. Primary aerosols emitted into the air as a result of mechanical processes such as wind erosion of soils to produce mineral aerosols or wave breaking to produce sea salt aerosol are large and known as coarse mode aerosols. These aerosols can have diameters of $10\mu m$ or more. Source regions of dust on a global scale include deserts (e.g., the Sahara in North Africa, Gobi in Mongolia and northern China, Mojave in southeastern California) and regions where foliage has been cleared by biomass burning and plowing. Deserts are continuously expanding due to land clearing and erosion on desert borders. Up to half of all wind-driven soil-dust emission worldwide may be anthropogenic.

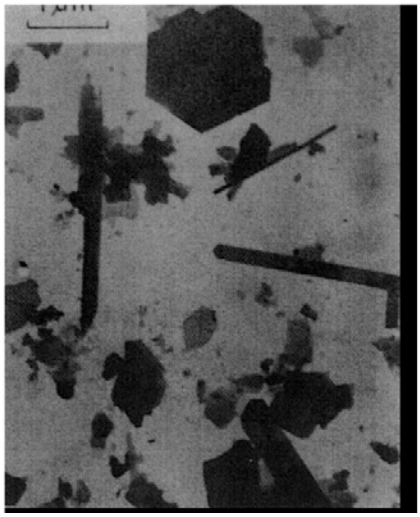

Figure 1.3: Scanning electron photograph of dust particles (Alexander and Kokhanovsky 2008).

Smoke aerosols (SMA) originate due to forest, grass, and other types of fires. Fires produce around 5 000 000 tons of particulate matter per year (Alexander and Kokhanovsky 2008). This is a small number as compared to the load of other aerosols. However, it has important local effects (e.g., as a cause of human, animal, and plant diseases; the reduction of visibility; and the changing of the heat balance) and an effect on global climate due to generally larger values of light absorption by smoke aerosol (e.g., black carbon) as compared to other aerosol species. The problem of black carbon influences on the planetary radiative budget is a hot topic in modern research. In particular, it has been found that aerosols transported to the Arctic from highly polluted areas in Europe can lead to a decrease in the planetary albedo (e.g, due to atmospheric absorption effects and also due to increased absorption of polluted snow and ice). Dirty snow modifies planetary albedo and makes an important contribution to the global warming of the planet.

Combustion processes produce tremendous numbers of small particles with radii below $0.1\mu m$. They also produce particles in the accumulation mode ($0.11\mu m$) , and giant particles with radii above $1\mu m$. The number of particles with radii above $0.5\mu m$ is relatively low. This means that particles of smoke can easily penetrate the respiratory system of humans leading to various health problems. Smoke aerosol has a large content of soot. Soot particles consist of aggregates with sizes generally greater than $1\mu m$ in diameter with many particles of a smaller size as well. The aggregates are formed from the coalescence of ultimate (or primary) particles, which are in the range 50 - 100 nm.

Volcanic aerosols (VA) originate due to emissions of primary particles and gases (e.g., gaseous sulfur) by volcanic activity. Most of the particles ejected from volcanoes (dust and ash) are water-insoluble mineral particles, silicates, and metallic oxides such as SiO_2, Al_2O_3 and Fe_2O_3, which remain mostly in the troposphere. Sulfur emissions from volcanoes have a longer lived effect on stratospheric aerosol loads. They occur mainly in the form of SO_2, even though other sulfur species may be present in the volcanic plume, predominantly SO_4^{2-} aerosols and H_2S. It has been estimated that the amount of SO_4^{2-} and H_2S is commonly less than 1% of the total, although it may in some cases reach $10-20\%$. Nevertheless, H_2S oxidizes to SO_2 in about 2 days in the troposphere or 10 days in the stratosphere. Calculations with global climate models suggest that the radiative effect of volcanic sulfate is only slightly smaller than that of anthropogenic sulfate, even though the anthropogenic SO_2 source strength is about five times larger. The main reason is that SO_2 is released from volcanoes at higher altitudes and has a longer residence- time than anthropogenic sulfate. Sulfate aerosol

Figure 1.4: St Helens erupting on May 18, 1980. Source: NASA

leads generally to cooling of a climate system. Therefore, there are theoretical studies with respect to the possibility of artificial production of this aerosol in the stratosphere with the aim of slowing down the current global warming trends (Alexander, Dr. and Kokhanovsky,A. (2008))..

Biological aerosols (BA) are characterized by the extreme particle size range and enormous heterogeneity. Biological material is present in the atmosphere in the form of pollens, fungal spores, bacteria, viruses, insects, fragments of plants and animals, etc. The volumetric concentration of bioaerosols depends on the season, location, and height of the sampling volume with smaller values at higher altitudes and in winter time (e.g., at high latitudes). Bioaerosols can occupy up to 30 percent of the total atmospheric aerosol volume at a given location (especially in remote continental areas). Their concentrations are at least three times smaller in remote marine environments. Nevertheless, bioaerosols produced inland can travel very long distances owing to their low density.

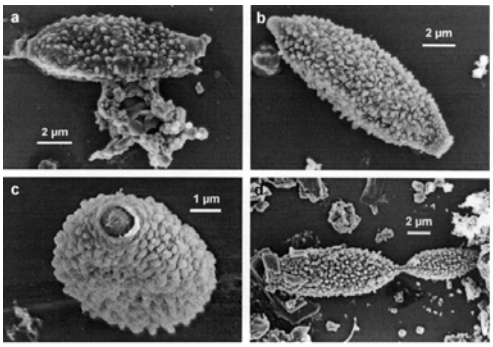

Figure 1.5: Scanning electron photographs of conidia of fungi species C. herbarum (Wittmack et al., 2005).

Secondary aerosol (SA) originates in the atmosphere due to gas-to-particle conversion. This aerosol is composed of mostly sulfates and nitrates. Also various organic substances (originating, for example, from gases emitted by plants) can make a large contribution in the total aerosol mass (Seinfeld and Pandis, 1997). In particular, SO_2 is oxidized to H_2SO_4 and the rate of conversion is influenced by the presence of heavy metal ions (e.g., Fe, Mn, V). The generated particles are mostly of spherical shape. Some of proposed reactions are given below:

$$SO_3 + H_2O \rightleftharpoons H_2SO_4$$

$$NO + O_2 + H \rightarrow HNO_3;$$

$$SO_2 + C_2H_2 + allene \rightarrow C_3H_4S_2O_3$$

$$NO_2 + hydrocarbons + photochemistry \rightarrow organic \quad nitrates;$$

$$SO_2 + alkanes \rightarrow sulfinilic \quad acid;$$

$$O_3 + olefines \rightarrow organic \quad particles$$

Anthropogenic aerosol (AA) consists of both primary particles (e.g., diesel exhaust and dust) and secondary particles formed from gaseous anthropogenic emissions. Secondary liquid particles are quite small and their shapes can be approximated by spheres. Anthropogenic aerosols contribute about 10percent of the total aerosol loading. However, these emissions did not occur in the pre-human era. The influence of this small (but growing) contribution on the climate system is not exactly known and must be assessed in future research.

1.3 Radiative and Climatic Effects of Aerosols

Aerosols scatter and absorb shortwave (solar) and longwave (thermal IR) radiation, thereby perturbing the energy budget of the Earth/atmosphere system and exerting a direct radiative forcing. Here the radiative forcing, RF, indicate a change in the radiative energy budget of the Earth's climate system due to an external perturbation or to the introduction of an agent, for example the aerosols or the greenhouse gases.

Aerosols also act as cloud condensation and ice nuclei, thereby modifying the microphysics, the radiative properties, and the lifetime of clouds. The aerosol indirect effect is usually split into two effects: the first indirect effect, whereby an increase in aerosols causes an increase in droplet concentration and a decrease in droplet size for fixed liquid water content, and the second indirect effect, whereby the reduction in cloud droplet size affects the precipitation efficiency, tending to increase the liquid water content, the cloud lifetime, and the cloud thickness.

There is also a semi-direct effect due to aerosols: the absorption of solar radiation by aerosols leads to a local heating in the atmosphere, which can suppress cloud cover. The local heating may simply lead to the evaporation of clouds, or may stabilize the atmosphere reducing cloud formation. A reduction of low clouds leads to a reduction of planetary albedo (since low clouds scatter solar radiation back to space) and a warming of climate. The effect of a particular aerosol type in terms of the direct RF can be positive, if it causes more radiation to be absorbed, thus leading to a warming, or negative, if it induces an increase in the outgoing radiation, thus causing a cooling.

1.4 Particle size distributions

The size distribution function of an aerosol is an important quantity to describe airborne particle populations. Since the properties and behavior of particles are highly dependent on particle size, it is not appropriate to describe the size of a particle population with a single parameter. Size distribution functions are used to describe how number or mass of particles are distributed over different particle sizes. Particle size distributions are analogous to non-normalized probability density functions. The number of particles per unit volume dN having diameters in the range D_p to D_p+dD_p is

$$dN = f_N(D_p)dD_p \tag{1.4.1}$$

where $f_N(D_p)$ is the number distribution function of aerosol particles. The total number of particles per unit volume, i.e. the total number concentration is

$$N_{tot} = \int_0^\infty f_N(D_p)dD_p \tag{1.4.2}$$

Similarly, the mass of particles per unit volume in the size range $[D_p, D_p + dD_p]$ is

$$dM = f_M(D_p)dD_p \tag{1.4.3}$$

where $f_M(D_p)$ is the mass distribution function. The total mass concentration is

$$M_{tot} = \int_0^\infty f_M(D_p)dD_p \tag{1.4.4}$$

In some contexts is it useful to express the distributions as functions of other quantities than diameter. For example, in (Voutilainen, A. et al. 2000) the size distribution was expressed as the function of the natural logarithm of the diffusion coefficient. In general, if the size distribution is needed to be expressed as the function of quantity z that is related to particle diameter D_p, the following relation must hold true

$$f_N(D_p)dD_p = f(z)dz \tag{1.4.5}$$

where $z = z(D_p)$. From (1.4.5) we obtain

$$f(z) = f(D_p)(\frac{dz}{dD_p})^{-1} \tag{1.4.6}$$

Since the size range of aerosol particles may cover several orders of magnitude, the size distribution function is usually expressed as a function of the logarithm of particle diameter. The dispersion of certain property of an aerosol is sometimes expressed with cumulative distribution functions. For instance, cumulative number and mass distributions give the number and mass concentrations of particles with diameter larger or smaller than D_p and they are obtained by integrating the size distributions $f_N(D_p)$ and $f_M(D_p)$ respectively. Cumulative number distributions are defined as

$$F_N(D_p) = \int_0^{D_p} f_N(D_p)dD_p \tag{1.4.7}$$

and

$$\bar{F}_N(D_p) = \int_{D_p}^{\infty} f_N(D_p) dD_p \tag{1.4.8}$$

Cumulative mass distributions $F_M(D_p)$ and $\bar{F}_M(D_p)$ can be obtained in similar way.

From Eqns. (1.4.7) and (1.4.8) one can observe that the total number concentration N_{tot} can be expressed as

$$N_{tot} = F_N(D_p) + \bar{F}_N(D_p) \tag{1.4.9}$$

The number distribution function can be obtained from the cumulative distributions as

$$f_N(D_p) = \frac{dF_N(D_p)}{dD_p} = -\frac{d\bar{F}_N(D_p)}{dD_p} \tag{1.4.10}$$

The above equations hold true for all kinds of size distribution functions.

Aerosol size distributions have been described and approximated with various parametric functions depending on the type of the aerosol. In the following some of the most commonly used parametric models are briefly reviewed.

1.4.1 Log-normal distribution

The number distribution of a particle population is often assumed to be a log-normal distribution, which is of the form

$$\frac{dN}{d\log D_p} = \frac{N_{tot}}{\sqrt{2\pi}\log\sigma_g} \exp\{-\frac{1}{2}(\frac{\log D_p - \log D_g}{\log\sigma_g})^2\}. \tag{1.4.11}$$

where N_{tot} is the total number concentration, D_g is the geometric mean diameter, which in this case equals to the median diameter D_{med}, and σ_g is the geometric standard deviation (Voutilainen, A. et al. 2000). Log-normal distributions have

been found to describe reasonably well aerosols covering a wide range of sizes and originating from a single source. The size distribution of a mixture of particles from several sources can be expressed as a combination of log-normal functions

$$\frac{dN}{d\log D_p} = \sum_i \frac{N_{tot,i}}{\sqrt{2\pi}\log\sigma_{g,i}} \exp\{-\frac{1}{2}(\frac{\log D_p - \log D_{g,i}}{\log\sigma_{g,i}})^2\}. \tag{1.4.12}$$

Log-normal functions can be used also for the representation of mass distributions.

1.4.2 Normal distribution

Size distribution functions are usually skewed having a long tail at large particle sizes and thus they are described with log-normal functions. However, some aerosols, e.g. certain nearly mono-disperse test aerosols and some plant spores, have symmetrical size distribution that can be approximated closely with a normal distribution

$$\frac{dN}{dD_p} = \frac{N_{tot}}{\sqrt{2\pi}\sigma} \exp\{-\frac{1}{2}(\frac{D_p - \bar{D}_p}{\sigma})^2\}, \tag{1.4.13}$$

where $\bar{D}_p$ is the mean particle diameter and σ is the standard deviation. A problem associated with the use of normal distributions is the fact that due to the symmetry normal distributions allow the presence of particles with negative diameters.

1.4.3 Junge power-law distribution

The number distribution of atmospheric aerosols is sometimes approximated with the Junge power-law distribution that can be expressed as

$$\frac{dN}{d\log D_p} = \frac{a}{D_p^b}, \tag{1.4.14}$$

where a is a positive constant and the exponent b has value of about 3. The Junge distribution has been applied to atmospheric aerosols on the size range from about $0.1\mu m$ to $100\mu m$. A drawback is that it can not be used to describe small particle sizes.

Chapter 2

Optical Properties of Tropospheric Aerosols

2.1 Introduction

Light can be scattered or absorbed by aerosol particles suspended in the terrestrial atmosphere. The processes of light scattering dominate over the processes of absorption in the visible. However, absorption of light cannot be ignored. It influences the total radiation balance considerably. The reduction in the intensity of a direct beam during its propagation through an aerosol medium is determined simultaneously by absorption and scattering processes. The sum of total light scattering in all directions and absorption is called extinction. Energy, which is absorbed by particles, is not contained in them indefinitely, but rather radiates at larger wavelengths (emission).

Light is composed of the superposition of electromagnetic waves having very high frequencies. To simplify, usually the idealized problem of a plane electromagnetic wave interaction with a single aerosol particle is considered under the assumption that an aerosol particle has a spherical shape. Then the electromagnetic field can be calculated both inside a particle (this is needed for the estimation of electromagnetic

energy absorption effects) and at an arbitrary distance from a scatterer. The Mie theory is based on the assumption of particles of spherical shape and homogeneous composition, which is not true for the largest aerosol types. Nevertheless, it is far the most used, since it can be applied to the entire range of dimensions of the particles

2.2 The Radiative Transfer Equation for a Plane-Parallel Atmosphere

2.2.1 Radiance and Irradiance

The fundamental quantity defining the radiation field is the specific intensity, or simply intensity, of radiation. Consider the light beam travelling in directions confined to an element of solid angle $d\Omega$, across an element of area $d\sigma$ orthogonal to the beam and during a time dt, in the frequency range $[\nu, \nu + d\nu]$. The radiant energy flux dE_ν associated to the light beam is expressed in terms of the intensity I_ν by

$$dE_\nu = I_\nu d\sigma d\nu d\Omega dt \tag{2.2.1}$$

If instead, the intensity orthogonal to an arbitrarily oriented surface element dA is considered, then the projection of $d\sigma$ onto dA has to be taken into account. If the angle between the direction considered and the normal to $d\sigma$ is θ then expression (2.2.1) becomes

$$dE_\nu = I_\nu cos\theta d\sigma d\nu d\Omega dt \tag{2.2.2}$$

The angular direction of the radiation is specified in terms of the polar angle θ and the azimuthal angle φ. The intensity I_ν is a function of spatial and temporal coordinates, of the direction, and of the frequency. Under the assumption of a stratified atmosphere, which is horizontally homogeneous, the physical quantities may vary

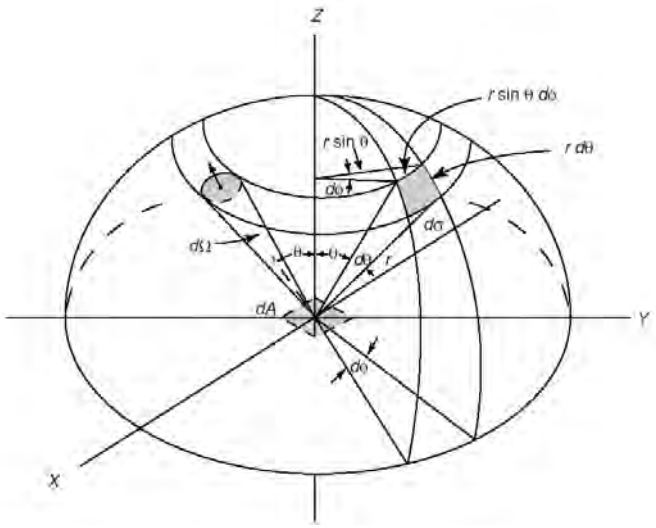

Figure 2.1: Illustration of a differential solid angle and its representation in polar coordinates.

only in the vertical dimension, z; this approximation is also known as a plane parallel atmosphere.

2.2.2 Equation of Radiative transfer

Radiation and matter have the following forms of interactions: scattering, absorption, and emission. The extinction of radiation due to traversing an infinitesimal increment of path is linearly proportional to the amount of matter along the path

$$\frac{dI_\nu}{ds} = -k_\nu \sigma_\nu I_\nu \tag{2.2.3}$$

where the extinction coefficient of the medium, k_ν, and σ_ν local density of the medium. Extinction includes all processes which reduce the radiant intensity. These processes include absorption and scattering which removes photons from the beam. Similarly the emission of radiation is also proportional to the amount of matter along the path

$$\frac{dI_\nu}{ds} = k_\nu \sigma_\nu S_\nu \tag{2.2.4}$$

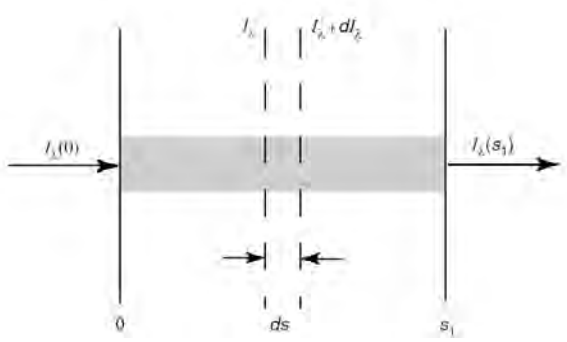

Figure 2.2: Extinction and emission of radiant intensity in traversing a medium

where S_ν is known as the source function. Emission includes all processes which increase the radiant intensity. These processes include thermal emission and scattering which adds photons to the beam. Extinction and emission are linear processes, and thus additive. Since they are the only two processes which alter the intensity of radiation (see Fig. 2.2),

$$\frac{dI_\nu}{ds} = k_\nu \sigma_\nu (-I_\nu + S_\nu) \tag{2.2.5}$$

This is the equation of radiative transfer in its simplest differential form.

2.2.3 Beer-Bouguer-Lambert Law

Consider a direct light beam from the sun, which covers the wavelengths from about 0.2 to $5\mu m$. Emission contributions from the earthatmosphere system can be generally neglected. Moreover, if the diffuse radiation produced by multiple scattering can be neglected, then Eqn. (2.2.5) reduces to the following form:

$$\frac{dI_\nu}{k_\nu \sigma_\nu ds} = -I_\nu \tag{2.2.6}$$

Let the incident intensity at $s = 0$ be $I_\lambda(0)$. Then the emergent intensity at a distance s away as shown in Fig. 2.2 can be obtained by integrating Eqn. (2.2.6) and is given by

$$I_\lambda(s_1) = I_\lambda(0) \exp(-\int_0^{s_1} k_\lambda \sigma_\nu ds) \tag{2.2.7}$$

Assuming that the medium is homogeneous, so that k_λ is independent of the distance s, and defining the path length

$$\mu = \int_0^{s_1} \sigma_\nu ds \tag{2.2.8}$$

Eqn. (2.2.7) can be expressed by

$$I_\lambda(s_1) = I_\lambda(0) e^{k_\lambda \mu} \tag{2.2.9}$$

This is known as Beers law or Bouguers law or Lamberts law, referred to here as the Beer-Bouguer-Lambert law, which states that the decrease in the radiant intensity traversing a homogeneous extinction medium is in accord with the simple exponential function whose argument is the product of the mass extinction cross section and the path length.

2.2.4 Angstrom Parameters

Although the chemical composition of aerosols and their size distributions are governed by a number of complex and not-well-understood processes, the resulting spectral aerosol extinction coefficient $k_{ext} = N\bar{C}_{ext}$, where N is the number of particles in a unit volume and $C_{ext} = C_{abs} + C_{sca}$ is the extinction cross-section (the overbar means averaging with respect to the aerosol size distribution), is often governed by the following simple analytical equation:

$$k_{ext} = b\lambda^{-\alpha} \tag{2.2.10}$$

where α is called the Angstrom parameter and b gives the value of the aerosol extinction coefficient at the wavelength $1\mu m$, if the wavelength λ is expressed in micrometers. It follows from this formula that

$$\ln k_{ext} = \ln b - \alpha \ln \lambda \tag{2.2.11}$$

The spectral aerosol optical depth τ measures extinction between different layers in the vertical. The optical depth between two levels $z_2 > z_1$ is given by the Beer-Lamberts Law as

$$\tau_\nu(z_1, z_2) = \int_{z'=z_1}^{z'=z_2} k_\nu dz'. \tag{2.2.12}$$

The Angstrom extinction law can also be presented in the following form:

$$\tau(\lambda) = \beta\lambda^{-\alpha} \tag{2.2.13}$$

where β is the turbidity and α is Angstrom exponential coefficient, β is related to the amount of aerosol present in the atmosphere while α is related to the size distribution of aerosol. α yields information on the predominant size of suspended particles. Like many other climatic variables, β and α can vary throughout an individual day simply because of change in temperature that cause evaporation or condensation of moisture in the atmosphere. These changes can increase or decrease the value of these parameters. The Ångstrom turbidity coefficient β owes a positive correlation with the atmospheric turbidity. The higher the turbidity, the more aerosol present in the atmosphere, where it usually has a value roughly between $0 \sim 0.5$. The Ångstrom exponent α is inversely proportional to particle size, i.e. the lower the value of α, the higher the proportion of bigger particles and vice versa. The value of α is normally between $0 \sim 4$. The closer it is to four the more Rayleigh scattering present; and the

closer it is to zero the more Mie scattering present. Angstrom found that the value of α is close to 1.3 for the average continental aerosols. The Ångstrom exponent appears to be a better indicator of aerosol size than the effective radius when the aerosol has a complicated size distribution (i.e., bi-mode or multi-mode size distribution).

2.2.5 Atmospheric Optical Depth

Aerosol optical and microphysical characteristics can be deduced from the analysis of solar light scattered or attenuated by the atmosphere using instruments placed on the ground, a ship, an aircraft or a satellite. The ground-based active or passive remote sensing techniques based on the analysis solar light (like it is not the case for active techniques).

The most common passive technique involves the measurement of the transmitted direct solar light beam. The direct-beam solar spectral irradiance $I(\lambda)$ can be expressed as the product of the extraterrestrial spectral irradiance $I_0(\lambda)$ and the atmospheric transmittance $T(\lambda)$, as

$$I(\lambda) = I_0(\lambda)\gamma T(\lambda) \tag{2.2.14}$$

where γ is the earth-sun distance correction factor (Osterwald, 2000)and given by

$$\begin{aligned} \gamma \quad &= 1.00011 + 3.4221 * 10^{-2}\cos(A_d) + 1.28 * 10^{-3}\sin(A_d) \\ &\quad +7.19 * 10^{-4}\cos(2A_d) + 7.7 * 10^{-5}\sin(2A_d) \end{aligned} \tag{2.2.15}$$

The day angle A_d is equal to $A_d = (J_d - 1)\frac{2\pi}{365}$ where J_d is the Julian day of the year.

Bouguers law expresses transmittance in terms of the monochromatic extinction optical thickness $\kappa(\lambda)$ as

$$T(\lambda) = \exp[-\kappa(\lambda)] \tag{2.2.16}$$

The extinction optical thickness, which we simply refer to as optical depth, is the product of a monochromatic attenuation coefficient $k(\lambda)$ and the optical pathlength or air mass m as:

$$\kappa(\lambda) = k(\lambda)m \tag{2.2.17}$$

Note that this attenuation coefficient is sometimes called the optical depth in the vertical directionthis is not the quantity we are calling optical depth. For direct-beam solar spectral irradiance, the optical path is through the atmosphere from the sun to the receiver site.

The total optical depth is simply a sum of the various scattering and absorber species:

$$\tau(\lambda) = \sum_i \kappa_i(\lambda) = \tau_R(\lambda) + \tau_A(\lambda) + \tau_{O_3}(\lambda) + \tau_{H_2O}(\lambda) \tag{2.2.18}$$

where the subscripts R, A, O_3 and H_2O refer to Rayleigh (molecular) scattering, aerosol scattering, ozone absorption, and the water vapor continuum. LOWTRAN expresses optical depth as a function of an absorption coefficient $C_i(\lambda)$ and an equivalent absorber amount X_i (which includes the optical pathlength)

$$\kappa_i(\lambda) = C_i X_i \tag{2.2.19}$$

2.2.6 Scattering

Scattering occurs when matter reflects off a photon without absorption. The direction of the photon after the interaction is usually not the same as the incoming direction.

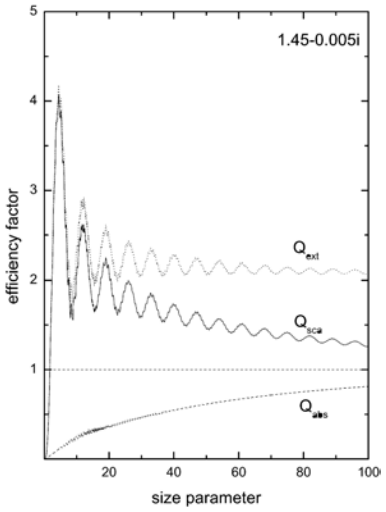

Figure 2.3: Dependence of Mie efficiency factors on the size parameter x at the refractive index 1.45 - 0.005i.

The theoretical description of light scattering by atmospheric aerosol is much more complex as compared to absorption and extinction. This is related to the fact that it is not enough just to have information on the aerosol scattering coefficient $k_{sca} = N\bar{C}_{sca}$, which is close to k_{ext} for atmospheric aerosol in most cases; also it is important to understand the angular distribution of scattered energy for a given local volume of an aerosol medium.

The dependence of scattering efficiency factor Q_{sca} and also absorption and extinction efficiency factors Q_{abs}, Q_{ext} on the size parameter are shown in Fig. 2.3 at $n = 1.45 - 0.005i$. For small size parameters, the absorption is small and $Q_{sca} \approx Q_{ext}$. However, with the growth of particles, Q_{abs} increases and Q_{sca} deviates from Q_{ext}. The scattering efficiency factor reaches its asymptotic value $Q_{sca} = 1 + r$ from above as $x \to \infty$. Oscillations on curves are due to interference of electromagnetic waves (e.g., diffracted and transmitted). Oscillations damp with the increase of absorption.

These oscillations are difficult to observe for natural aerosols because the interference is destroyed by the polydispersity of particles and also because solar light is far away from an idealized coherent monochromatic incident beam assumed in calculations shown in Fig. 2.3. One can conclude from Fig. 2.3 the asymptotic regime ($Q_{abs} = 1-r$) is reached more quickly for the absorption efficiency factor as compared to the scattering efficiency factor. Clearly, it follows that $Q_{ext} = Q_{abs}+Q_{sca} \rightarrow 2$ from above as $x \rightarrow \infty$. Mie calculations show that Q_{ext} can be described by the following approximate equation in the vicinity of asymptotic: $Q_{ext} = 2(1 + x^{-2/3})$. Accurate estimate of Mie efficiency factors in the vicinity of the asymptotic regime are given by on the base of complex angular momentum theory (Alexander and Kokhanovsky, 2008)

The scattering regimes are:

Rayleigh scattering: $2\pi r/\lambda << 1$, applies to scattering by molecules and small aerosol particles;

Mie-Debye scattering: $2\pi r/\lambda \sim 1$, applies to scattering by aerosol and cloud particles;

Geometric optics: $2\pi r/\lambda >> 1$, applies to scattering by large cloud droplets.

Rayleigh Scattering

The sizes of atmospheric molecules are much smaller than the wavelengths of solar and IR radiation, and the scattering by atmospheric gases is well described by the Rayleigh scattering. In the Rayleigh scattering approximation, a molecule (or a small particle) is considered as an individual dipole. The intensity scattered by molecules

for unpolarized incident light is given by [Bucholtz, 1995]

$$I = \frac{I_0}{r^2}\alpha^2(\frac{2\pi}{\lambda})^4(1 + cos^2\Theta) \tag{2.2.20}$$

where r is the particles' radius and α is the polarizability, defined by

$$\alpha = \frac{3}{4\pi N}(\frac{m^2 - 1}{m^2 + 2}) \tag{2.2.21}$$

with N the number of molecules per unit volume and m the complex refractive index. The Rayleigh scattering intensity is inversely proportional to the fourth power of the wavelength. The Rayleigh scattering phase function for incident unpolarized radiation is

$$P(cos\Theta) = \frac{3}{4}(1 + cos^2\Theta) \tag{2.2.22}$$

Mie Scattering

The basic assumptions of the Mie theory are the spherical shape of the particles and their homogeneous composition. Mie scattering has no size limitations and converges to the limits of geometrical optics for large particles, and of Rayleigh scattering for $2\pi r/\lambda << 1$.

Mie theory calculates the scattered electromagnetic field at all points in the particle (called internal field) and at all points of the homogeneous medium in which the particle is embedded. For all practical applications in the atmosphere, light scattering observations are carried out in the far-field zone (i.e., at the large distances r from a particle). In the far-field zone the solution of the vector wave equation can be obtained as

$$\begin{bmatrix} E_l^s \\ E_r^s \end{bmatrix} = \frac{exp(-ikr + ikz)}{ikr} \begin{bmatrix} S_2 & S_3 \\ S_4 & S_1 \end{bmatrix} \begin{bmatrix} E_l^i \\ E_r^i \end{bmatrix} \tag{2.2.23}$$

where $k = \frac{2\pi}{\lambda}$, $exp(ikz)$ is the incident plane wave and $\frac{exp(-ikr)}{ikr}$ is the outgoing scattered wave. E_l^i and E_r^i are the parallel and perpendicular components of incident electrical field, and E_l^s and E_r^s are the parallel and perpendicular components of scattered electrical field, and $\begin{bmatrix} S_2(\Theta) & S_3(\Theta) \\ S_4(\Theta) & S_1(\Theta) \end{bmatrix}$ is the amplitude scattering matrix. For sphere $S_3(\Theta) = S_4(\Theta) = 0$ so that Eqn. (3.2.15) is the fundamental equation of scattered radiation including polarization.

$S_1(\Theta)$ and $S_2(\Theta)$ are the Mie scattering amplitudes, expressed by

$$S_1(\Theta) = \sum_{n=1}^{\infty} \frac{2n+1}{n(n+1)} [a_n \pi_n(cos\Theta) + b_n \tau_n(cos\Theta)] \tag{2.2.24}$$

$$S_2(\Theta) = \sum_{n=1}^{\infty} \frac{2n+1}{n(n+1)} [b_n \pi_n(cos\Theta) + a_n \tau_n(cos\Theta)] \tag{2.2.25}$$

where π_n and τ_n are the Mie angular functions, expressed as a function of the associated Legendre polynomials. a_n and b_n are coefficients for the scattered waves which must be determined from the boundary conditions at the surface of the sphere. From Mie theory it follows that the extinction cross section of a particle is

$$\sigma_e = \frac{4\pi}{k^2} Re[S_{1,2}(\Theta = 0^0)]. \tag{2.2.26}$$

From Eqns. (3.2.16) and (3.2.17) for $\Theta = 0^0$, the scattering amplitudes are given by

$$S_1(\Theta = 0^0) = S_2(\Theta = 0^0) = \frac{1}{2}(2n+1)(a_n + b_n) \tag{2.2.27}$$

Thus, extinction cross section is related to the scattering in the forward direction. The efficiency factors for extinction, scattering and absorption are defined as

$$Q_{e,s,a} = \frac{\sigma_{e,s,a}}{\pi a^2} \tag{2.2.28}$$

where πa^2 is the particle area projected into the plane perpendicular to the incident beam. Mie efficiency factors are derived from the Mie scattering amplitude:

$$Q_e = \frac{2}{(ka)^2}\sum_{n=1}^{\infty}(2n+1)Re[a_n + b_n] \tag{2.2.29}$$

$$Q_s = \frac{2}{(ka)^2}\sum_{n=1}^{\infty}(2n+1)[|a_n|^2 + |b_n|^2] \tag{2.2.30}$$

where $Q_a = Q_e - Q_s$.

For a given aerosol type with size distribution N(r) the extinction, scattering and absorption coefficients are then determined as

$$\sigma_{e,s,a} = \int_{r_1}^{r_2} Q_{e,s,a}(r)\pi r^2 \frac{dN(r)}{r\ln 10 d(\log r)}dr \tag{2.2.31}$$

From Eqns. (2.2.12) and (2.2.31) one can result in an integral equation that relates the aerosol optical depth and the aerosol size distribution which we discuss briefly on the next chapter.

Chapter 3

Aerosol Size Distribution Retrieval

3.1 Introduction

It is well known that the characteristics of aerosol particle size, which can be represented as a size distribution function in the mathematical formalism, say $n(r)$, play an important role in affecting the climate, so it is necessary to determine the size distribution function of the aerosol particle. Aerosol size distributions can be derived from measured aerosol optical properties, such as the wavelength dependence of aerosol optical depth (King et al. 1978), or backscattering or a combination of radiances scattered at different angles and optical depth spectra (Kuzmanoski et al 2007; Dubovik et al. 1995). These approaches yield integrated size distribution in a vertical column of an atmospheric layer. As no interaction with particles is involved, retrieval of aerosol size distributions from their optical properties has the advantage of giving information on size distributions in ambient conditions. The retrieved size distributions can be used to calculate the column integrated aerosol optical properties, needed as an input into radiative transfer codes.

3.2 Retrieval Formulism

Assuming that the atmospheric particulate can be modelled by equivalent sphere of known refractive index to the sufficient degree of accuracy, the integral equation which relates the optical depth to an aerosol size distribution can be written as

$$\tau_m(\lambda) = \int_0^\infty \int_0^\infty \pi r^2 Q_{ext}(r, \lambda, m) n(r, z) dz dr \tag{3.2.1}$$

where $n(r, z)dr$ is the height dependant aerosol number density in the radius range r to $r+dr$; m is the complex refractive index of the aerosol particles; λ is the wavelength of the incident illumination; and $Q_{ext}(r, \lambda, m)$ is the extinction efficiency factor from Mie theory. Performing the height integration, Eqn. (3.2.1) can be rewritten as

$$\tau_m(\lambda) = \int_0^\infty \pi r^2 Q_{ext}(r, \lambda, m) n(r) dr \tag{3.2.2}$$

where $n_c(r)$ is the unknown columnar aerosol size distribution (i.e. the number of particles per unit area per unit radius interval in a vertical column through the atmosphere).

The integral in Eqn. (3.2.2) can be replaced by a summation over coarse interval in r, each of which is composed of several subintervals as described by Herman et al.(1971) for the case of the angular distribution of scattered light of one wavelength. In order to examine the specific Kernel function, we let

$$n_c(r) = h(r) \cdot f(r) \tag{3.2.3}$$

where $h(r)$ is a rapidly varying function of r, while $f(r)$ is more slowly varying. Substitution of Eqn. (3.2.3) on to Eqn. (3.2.2) results in

$$\tau_m(\lambda) = \int_{r_a}^{r_b} \pi r^2 Q_{ext}(r,\lambda,m) h(r) f(r) dr \tag{3.2.4}$$

$$= \sum_{j=1}^{q} \int_{r_j}^{r_{j+1}} \pi r^2 Q_{ext}(r,\lambda,m) h(r) f(r) dr \tag{3.2.5}$$

where the limit of integration have been made finite with $r_1 = r_a$ and $r_{q+1} = r_b$.

If $f(r)$ is assumed constant within each coarse interval, a system of linear equations results which may be written as

$$g = Af + \varepsilon \tag{3.2.6}$$

where ε is an unknown error vector whose elements ϵ_i represent the deviation between measurement (g_i) and theory ($\sum_i A_{ij} f_j$). This deviation arises from quadrature and measurement error, as well as any uncertainties as to the exact form of the Kernel function [in this case $\pi r^2 Q_{ext}(r,\lambda,m)$].

Returning to Eqn. (3.2.4) it follows that the elements of Eqn. (3.2.6) are given as

$$g_i = \tau_m(\lambda_i) \qquad i = 1,2,3,.....,p \tag{3.2.7}$$

$$A_{ij} = \int_{r_i}^{r_{j+1}} \pi r^2 Q_{ext}(r,\lambda,m) h(r) dr \qquad j = 1,2,3,.....,q \tag{3.2.8}$$

$$f_j = f(\bar{r_j}) \qquad r_i \le r \le r_{i+1} \tag{3.2.9}$$

In terms of an integral over $x = \log r$, A_{ij} may be rewritten as

$$A_{ij} = \int_{x_j}^{x_{j+1}} K(x,\lambda_i) dx \tag{3.2.10}$$

where $K(x,\lambda) = \pi 10^{3x} Q_{ext}(10^x,\lambda,m) h(10^x) \ln 10$

Here we fixed that $h(r)$ takes the form of a Junge (1955) size distribution

$$h(r) = r^{-(v^*+1)} \tag{3.2.11}$$

with v^* assumed to have a value of 3.0

For a quadrature of equal division, the solution vector f is obtained by minimizing a performance function Q defined as

$$Q = \sum_{i=1}^{p} \epsilon_i^2 + \gamma \sum_{j=2}^{q-1} (f_{j-1} - 2f_j + f_{j+1})^2 \tag{3.2.12}$$

where γ is some non-negative Lagrange multiplier. Minimizing Q with respect to the unknown f_k coefficients, when γ equals zero is equivalent to making an unweighted least-squares fit to the data.

Since it is further known that some of the $\tau_m(\lambda)$ measurements are more precise than others, it is desirable to include that a priori information in the mathematical formalism for the case in which the measurements are correlated with known covariances σ^2_{gigj} a more general form of eqn. (3.2.12) would be

$$Q = \sum_{i=1}^{p} \sum_{j=1}^{p} C_{ij}^{-1} \epsilon_i \epsilon_j + \gamma \sum_{j=2}^{q-1} (f_{j-1} - 2f_j + f_{j+1})^2 \tag{3.2.13}$$

where C_{ij} is an element of the measurement covariance matrix C whose elements are given by $C_{ij} = \sigma^2_{gigj}$. Thus the minimum value of Q represents the statistical optimum estimate of f.

Following the method suggested by Twomey(1963) whereby the performance function is differentiated with respect to each of the f_k coefficients, a set of simultaneous equation results which may be written as

$$-\sum_{i=1}^{p} \sum_{j=1}^{p} C_{ij}^{-1} A_{ik} \epsilon_j + \gamma \sum_{j=1}^{q} H_{kj} f_j = 0 \qquad k = 1, 2, ..., q \tag{3.2.14}$$

where H_{kj} is an element of the smoothing matrix H defined by Twomey(1963) as

$$H = \begin{pmatrix} 1 & -2 & 1 & 0 & 0 & 0 & ... & 0 & 0 \\ -2 & 5 & -4 & 1 & 0 & 0 & ... & 0 & 0 \\ 1 & -4 & 6 & -4 & 1 & 0 & ... & 0 & 0 \\ 0 & 1 & -4 & 6 & -4 & 1 & ... & 0 & 0 \\ \vdots & ... & \ddots & \ddots & \ddots & \ddots & \ddots & \vdots & \vdots \\ 0 & ... & 0 & 1 & -4 & 6 & -4 & 1 & 0 \\ 0 & ... & 0 & 0 & 1 & -4 & 6 & -4 & 1 \\ 0 & ... & 0 & 0 & 0 & 1 & -4 & 5 & -2 \\ 0 & ... & 0 & 0 & 0 & 0 & 1 & -2 & 1 \end{pmatrix} \tag{3.2.15}$$

Eqn. (3.2.14) can be written in compact matrix form as

$$-A^T C^{-1} \epsilon + \gamma H f = 0 \tag{3.2.16}$$

where A^T is the transpose of A. Eliminating ϵ between eq. 3.2.6 and 3.2.16 leads to the solution

$$f = (A^T C^{-1} A + \gamma H)^{-1} A^T C^{-1} g \tag{3.2.17}$$

In Eqn. (3.2.17) A is the Kernel matrix, H is the smoothing matrix, g is the vector of optical depth and f is the size distribution array. This is the equation used to obtain the size distribution. The Lagrange multiplier, γ ensures that the algorithm will produce stable result. substituting the results of Eqns. (3.2.11) and (3.2.17) for h(r) and f(r) on Eqn. (3.2.3) the columnar size distribution can be written as

$$n_c(r) = r^{-4} \cdot f \tag{3.2.18}$$

This is the equation that we use finally to determine the columnar aerosol size distribution.

Chapter 4

Ozone

4.1 Source of Ozone

Ozone is a gas at room temperature that occurs naturally in our atmosphere. The gas is colorless with a pungent odor readily detectable at concentrations as low as 0.02 to 0.05 ppm (by volume), which is below concentrations of health concern. Most of it is concentrated in the ozone layer, a region located in the stratosphere several miles above the surface of the Earth. Although ozone represents only a small fraction of the gas present in the atmosphere, it plays a vital role by shielding humans and other life from harmful ultraviolet light from the Sun. Human activities in the last several decades have produced chemicals, such as chlorofluorocarbons (CFCs), which have been released into the atmosphere and have contributed to the depletion of this important protective layer.

4.2 Stratospheric Ozone Chemistry

The simplest treatment of ozone photochemistry is attributed to Sydney Chapman (1930), who proposed that the formation of "odd oxygen" $O_x(= O, O_3)$ is due to photolysis of molecular oxygen O_2 by solar radiation at wavelength shorter than 242

nm as shown in the reaction R1 to R5.

$O_2 + h\nu(\lambda < 242nm) \rightarrow O + O$ photolysis frequency (J_2) altitude dependant [R1]

$O + O_2 + M \rightarrow O_3 + M + 24Kcal/mol$ weakly temperature dependant (k_2) [R2]

$O_3 + h\nu(\lambda < 1140nm) \rightarrow O_2 + O$ photolysis frequency (J_3) altitude dependant [R3]

$O + O_3 + M \rightarrow 2O_2 + M + 94Kcal/mol$ temperature dependant (k_3) [R4]

$O + O + M \rightarrow 2O_2 + M + 118Kcal/mol$ [R5]

where the rate coefficient in parentheses characterize the speed of the individual reactions. Fast reaction [R2], where M is a mediator, and [R3] next lead to the rapid establishment of a steady state for the concentration of odd oxygen, counteracting its production by reaction [R1] occurs by reaction [R4]. These reactions result in the equilibrium of ozone number density:

$$[O_3] = [O_2]\sqrt{\frac{k_2 J_2}{k_3 J_3}[M]} \tag{4.2.1}$$

where $[O_3]$ and $[O_2]$ are the amount of ozone and oxygen respectively. In the reaction [R2], [R4] and [R5] M represents a background gas, which is involved absorbing the exceeding energy; the reactions [R2], [R4] and [R5] are exothermic and determine the strong temperature increase in the stratosphere.

According to Chapman's theory the formation of ozone is initiated by the UV photolysis of molecular oxygen [R1] which yield two oxygen atoms. Ozone is formed via three-body recombination of atomic oxygen with molecular oxygen [R2], which

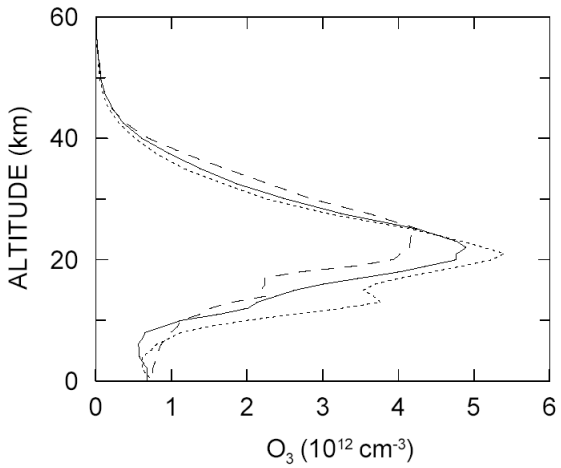

Figure 4.1: Vertical ozone profiles for the Standard U.S. (solid line), the Midlatitude summer (dashed line) and Midlatitude winter (dotted line) atmosphere (Meloni, 2000).

computes with the distraction of ozone via ([R3] and [R4]).

4.3 Distribution of ozone

Ozone is mainly produced in the stratosphere, since at higher altitudes the O_2 concentration is too low, while at lower altitudes the solar radiation with $\lambda < 242nm$ can not penetrate, due to O_2 and O_3 absorption. Fig. 4.1. shows the vertical ozone profile for the Standard U.S. atmosphere and for the Midlatitude winter and summer atmosphere.

The columnar amount of a gas can be expressed as the height of the column of unitary section occupied by the gas at standard pressure and temperature; 1 mm of height corresponds to 100 DU. The average total ozone distribution as a function of latitude and season, derived from the Total Ozone Mapping Spectrometer (TOMS)

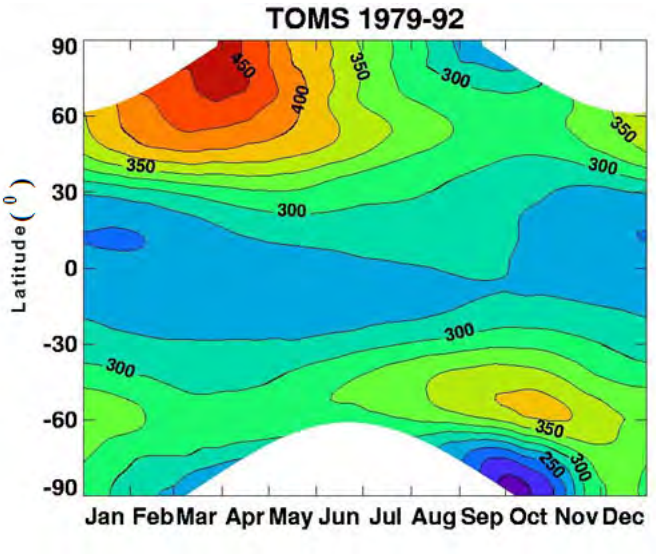

Figure 4.2: Latitudinal and seasonal distribution of total ozone in Dobson units. Values are averages over the TOMS measurements for the years 1979-1992. Source: NASA

over the years 1979-1992, is shown in Fig.4.2. Values are typically lower in the tropics throughout the year and highest during the spring at mid- and high latitudes but with clearly lower levels in the southern polar region. This distribution is far different from the one that is expected on the base of the Chapman model, which predicts largest concentrations in the equatorial region, where photochemistry is more intense and insolation is strongest. The discrepancy is due to the fact that firstly the Chapman model does not take into account the effect of circulation on the ozone transport. The maxima at high latitudes are due to O_3 transport from the high equatorial stratosphere, where the ozone production is strongest, to the middle and low stratosphere in the polar regions, where O_3 is relatively inert. The polar maximum is stronger in the Northern than in the Southern hemisphere, due to the different horizontal mixing caused by the different proportion of land and ocean. Secondly in neglecting additional chemical ozone destroying cycles. In these cycles free radicals

act catalytically, i.e. they remain unchanged while destroying ozone. The importance of a catalytic cycle is determined by the concentration of the involved radical, the number of cycles that are possible during the lifetime of the radical. In those catalytic cycles the radical destroys ozone without being removed.

$$\begin{array}{rl} & X + O_3 \rightarrow XO + O_2 \\ & XO + O \rightarrow X + O_2 \\ \hline net & \quad O + O_3 \rightarrow 2O_2 \end{array} \tag{4.3.1}$$

with OH, NO, Cl or Br act as radicals X. Precursor molecules of the radicals generally originate from the earth's surface, and by photo- dissociation they transform into reactive radicals in the stratosphere. CH_4 and H_2O for example, can be converted into OH , and N_2O in to NO. Both CH_4 and N_2O are produced in enormous quantity by microorganisms. Cl and Br are produced from anthropogenically injected $CFCs$ and halogns.

4.4 Absorbtion band of Ozone

Absorption of ultraviolet, visible and near-IR radiation in the gaseous atmosphere is primarily due to H_2O, O_3, and CO_2, as shown in Fig. (4.3).

Absorption of UV radiation in the gaseous atmosphere is primarily due molecular oxygen O_2 and ozone O_3. The absorption of ozone in the solar spectral region is due to electronic transitions. The strongest ozone bands are the Hartley bands, which cover the region from 2000 to 3000 $\mathring{A}$ and are centered at 2553$\mathring{A}$. The absorption of solar flux in these ozone bands takes place primarily in the upper stratosphere and in the mesosphere. The weak bands between 3000 and 3600$\mathring{A}$ have more structure

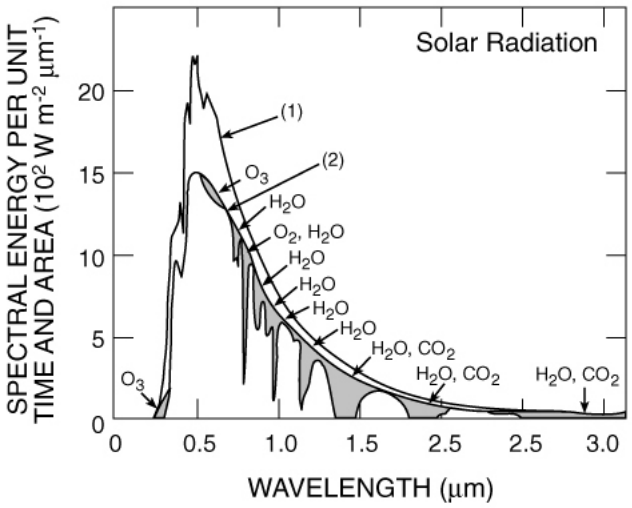

Figure 4.3: Spectrum of solar radiation (1) outside the Earths atmosphere and (2) at sea level for clear sky conditions. The shaded area represents the energy absorbed by the indicated gases in a clear atmosphere.

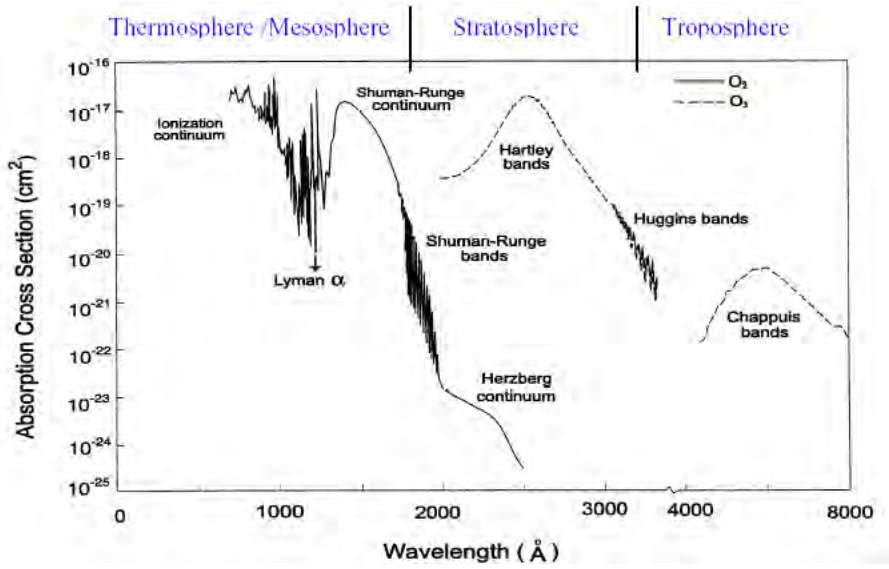

Figure 4.4: Spectral absorption cross-sections of O_2 (solid line) and O_3 (dashed line).

and are called the Huggins bands. Ozone also shows weak absorption bands in the visible and near-IR regions from about 4400 to 11,800$\mathring{A}$. These bands are referred to as Chappuis bands. The absorption coefficients in these bands are slightly dependent upon temperature. They have been measured by a number of earlier researchers (Liou, 2002).

Chapter 5

Materials and Methodology

5.1 Instrument

The MICROTOPS II (MICRO-processor based Total Ozone Portable Spectrometer), is a compact, portable and hand-held multi-band sunphotometer capable of measuring the total ozone column and optionally the water vapor column (also called precipitable water) as well as aerosol optical thickness at 1020nm.

The instrument is equipped with 5 accurately aligned optical collimators, capable of a full field view of 2.5^0. Internal baffles are also integrated into the device to eliminate internal reflections. Each channel is fitted with a narrow-band interference filter and a photodiode suitable for the particular wavelength range. The collimators are encapsulated in a cast aluminum optical block for stability.

A sun target and pointing assembly is permanently attached to the optical block and laser-aligned to ensure accurate alignment with the optical channels. When the image of the sun is centered in the bulls-eye of the sun target, all optical channels are oriented directly at the solar disk. A small amount of circumsolar radiation is also

captured, but it makes little contribution to the signal.

Radiation captured by the collimator and bandpass filters radiate onto the photodiodes, producing an electrical current that is proportional to the radiant power intercepted by the photodiodes. These signals are first amplified and then converted to a digital signal by a high resolution A/D converter. The signals from the photodiodes are processed in series. However, with 20 conversions per second, the results can be treated as if the photodiodes were read simultaneously.

5.2 Data Collection Site

The study area, Addis Ababa, extends over $8^0 55^{'}$ to $9^0 6^{'} N$ and $38^0 10^{'}$ to $39^0 05^{'} E$, which is the capital city of Ethiopia. The measurements has been carried out at Addis Ababa university, science faculty, at observatory located at $09^0 01^{'} N$ and $38^0 45^{'} E$ and an altitude of 2445m a.m.s.l. Data has been collected at the wave length 305, 312, 320, 936, and 1020 nm using Microtops II sunphotometers for the first time.

The sampling period is from March 20 to May 10, 2009. This time period is dry season in the study area, The lowest temperature occurred in the morning at about 7:00 LT is around $20^0 C$, and the maxima in the afternoon at 13:00 LT is around $27^0 C$. Of all the days, the temperature showed a similar trend with little difference from day to day. Relative humidity was inversely coupled to the diurnal temperature with maxima in the early morning and minima around 12:00 LT. High temperature and low relative humidity were observed during our sampling period.

5.3 Methodology

5.3.1 Measurements of ozone and precipitable water content

Total columnar ozone (TCO), an equivalent to the thickness of pure ozone layer at standard temperature and pressure, is measured by recording the differential absorption of solar light intensity at wavelengths in the UV region (305 and 320.0 nm). The measurement at third wavelength (312 nm) is used to correct for particulate scattering and stray light (Devara et al., 2001). On the other hand, precipitable water content (PWC) measurement is based on a pair of radiometric measurements in near-IR band. The estimation of PWC was made by following the differential optical absorption method applied to the irradiance data archived at 936 and 1020 nm channels. The 936 nm channel is located in the strong water vapor absorption band whereas 1020 nm channel has negligible water vapor absorption but it is affected by aerosol scattering.

5.3.2 Determination of aerosol optical depth from the measured signal

Total optical depth in a vertical air column at wavelength λ was determined from the Beer-Lambert-Bouguer law, expressing total attenuation of direct solar beam through the atmosphere, in the form of

$$I(\lambda) = I_0(\lambda) \exp[-\tau_t(\lambda)] \tag{5.3.1}$$

where $I(\lambda)$ is the monochromatic solar irradiance reaching at the instrument detector, $I_0(\lambda)$ is the irradiance measured by the our MICROTOPS II if it were at the top-of-atmosphere, $\tau_t(\lambda)$ is the total optical depth in slant path.

$I_0(\lambda)$ is determined from the irradiance incident at the top-of-atmosphere (TOA), data obtained from (http://eosweb.larc.nasa.gov/cgi-bin/see/daily.cgi.) and the calibration factor (calfac) of our MICROTOPS II as

$$I_0(\lambda) = TOA \cdot calfac \tag{5.3.2}$$

where the $calfac$ for 305 nm, 312 nm, 320nm, 936 nm and 1020 nm optical channels are 0.03215, 0.144504, 0.289, 0.6287 and 0.6163 respectively.

The spectral aerosol optical depth $\tau_A(\lambda)$ in slant path was calculated from the total optical depth $\tau_t(\lambda)$ by accounting for Rayleigh scattering $\tau_R(\lambda)$ and the contribution of gas absorbers (Madhavi and Badrinath, 2004)

$$\tau_A(\lambda) = \tau_{total}(\lambda) - \tau_R(\lambda) - \tau_{O_3}(\lambda) - \tau_{H_2O}(\lambda) \tag{5.3.3}$$

where $\tau_R(\lambda) = \frac{P}{P_0} \times 0.008735 \times \lambda^{-4.08}$ is Rayleigh scattering optical depth, P is the actual air pressure in hpa and $P_0 = 1013.25hpa$, $\tau_{O_3}(\lambda) = \alpha(\lambda)\Omega(Du)$ is ozone optical depth, $\alpha(\lambda) = (2.1349x10^{19}) \exp(-0.14052\lambda)$ is ozone spectral absorbtion coefficient, derived by fitting the ozone cross sections derived by Molina, L. T., and Molina. M. J. (1986). $\Omega(Du)$ is the measured total columnar ozone in Dobson unit. $\tau_{H_2O}(\lambda) = C_{H_2O}(\lambda)X(cm)$ is water vapor optical depth where $X(cm)$ is measured precipitable water content and $C_{H_2O}(\lambda)$ is absorption coefficients of water vapor tabular values for each wavelength taken from Osterwald and Emery (2000). For 936 nm optical channel we use the radiation transfer model relationship. The radiation transfer model relates the AOD at 1020 nm (τ_1) and AOD at 936 nm (τ_2) as $\tau_2 = 1.16\tau_1$.

5.3.3 Determination of atmospheric turbidity

Aerosol optical depth offers itself as a possible measure of atmospheric turbidity. The most frequently used turbidity coefficient is obtained by Angstrom (Madhavi and Badrinath, 2004):

$$\tau_A(\lambda) = \beta\lambda^{-\alpha} \tag{5.3.4}$$

where β is the Angstrom turbidity coefficient, α is the Angstrom exponent (wavelength exponent) and wave length λ is in μm.

The equation can be facilitated by useing its linearized form as

$$\ln \tau_A(\lambda) = \ln \beta - \alpha \ln \lambda \tag{5.3.5}$$

Simultaneous computation at different wavelength yields

$$\alpha = -\ln(\tau_{\lambda_1}/\tau_{\lambda_2})/\ln(\lambda_1/\lambda_2) \tag{5.3.6}$$

β is found by substituting the value of α on Eqn. (5.3.4)

5.4 Source of Errors

The instruments precision is $1-2\%$. Error in the MICROTOPS-II measurements can be caused by poor pointing at the sun and presence of optically thin sub-visible cloud/haze layers in the sensing region. Errors on the final results may caused due to these measurement errors and approximations on the calculation of aerosol optical depth.

5.4.1 Air mass back trajectory using HYSPLIT model

The back-trajectories trace the history of air parcels, which influenced the aerosol characteristics at the location of observation, back in time. For exploring the possible

reasons for the extreme AODs and their association with PWC as a consequence of aerosols loading at the site, the Hybrid Single-Particle Lagrangian Integrated Trajectory (HYSPLIT) model was used. To understand long range transport of aerosols with the air masses in the region, back trajectories have been able to indicate the original sources of air masses. Five days back trajectories obtained from the NOAA HYSPLIT model (http://www.arl.noaa.gov/ ready/hysplit4.html) ending at Addis Ababa (09.033N, 38.7E) at 12:00 LT at different altitudes of 500, 1000 and 1500m above the ground level (AGL) were analyzed for each days.

Chapter 6

Result and Discussion

6.1 Day-to-day Spectral Variation of Aerosol Optical Depth

Knowledge on the spectral dependence of AOD is important for adequately modelling the effects of aerosols on the radiation budget of the earth atmosphere system or for accurately retrieving the aerosol optical parameters from satellite-remote sensors. The wavelength dependence of AOD varies between different aerosol types because of their different physical and chemical characteristics. Using the Beer-Lamberts law discussed in Section (5.3.2), we calculated the aerosol optical depth at a wavelength range of 305.5 nm - 1020 nm. Figs. 6.1 shows the daily variations in spectral distribution of AOD observed on clear sky days from March 20 to May 10, 2009. The spectral variation of aerosol optical depth exhibits high value at smaller wavelengths and vice-versa as expected from the Mie theory (i.e. the extinction coefficient is inversely proportional to the square of the wavelength ($Q_{sca}\ \alpha\ \frac{1}{\lambda^2}$). It is also evident from Figs. 6.1 a remarkable higher AOD is observed on 29 March, 2009 at 305.5nm suggesting the fine mode particle loading was observed to be high over the study area during this day. This is attributed to the long range transported fine dust aerosols

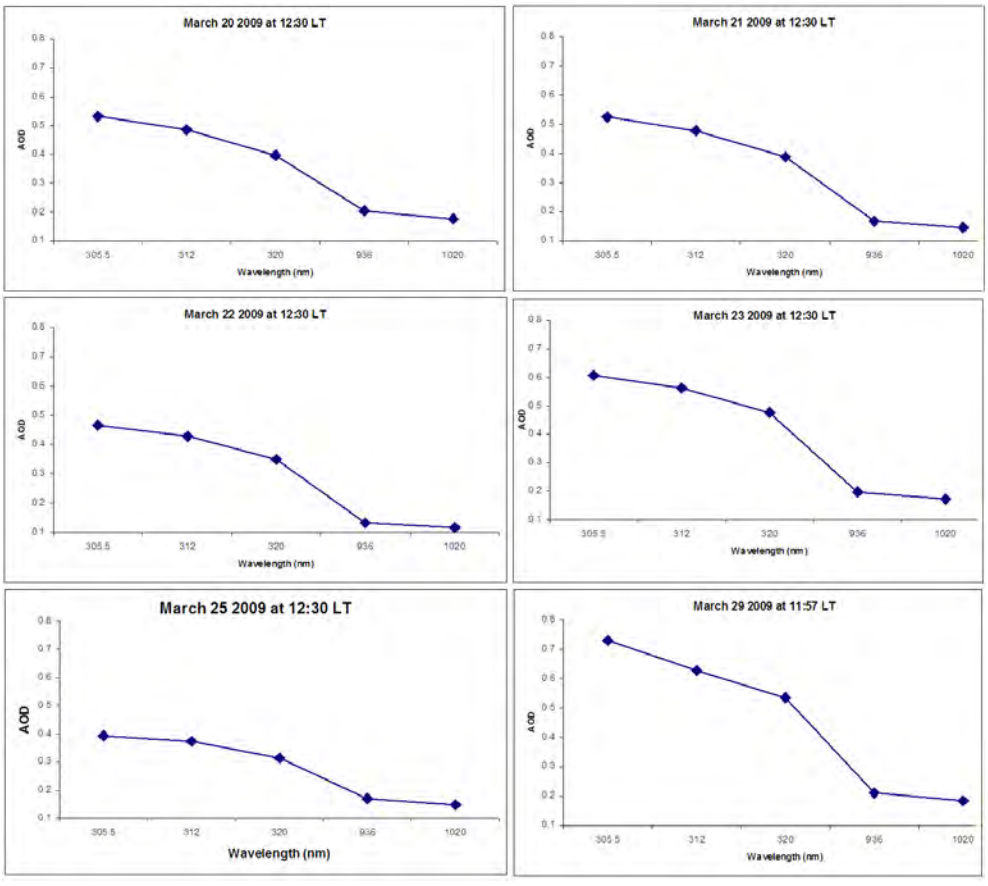
March 20 2009 at 12:30 LT
March 21 2009 at 12:30 LT
March 22 2009 at 12:30 LT
March 23 2009 at 12:30 LT
March 25 2009 at 12:30 LT
March 29 2009 at 11:57 LT
AOD
Wavelength (nm)
305.5
312
320
936
1020

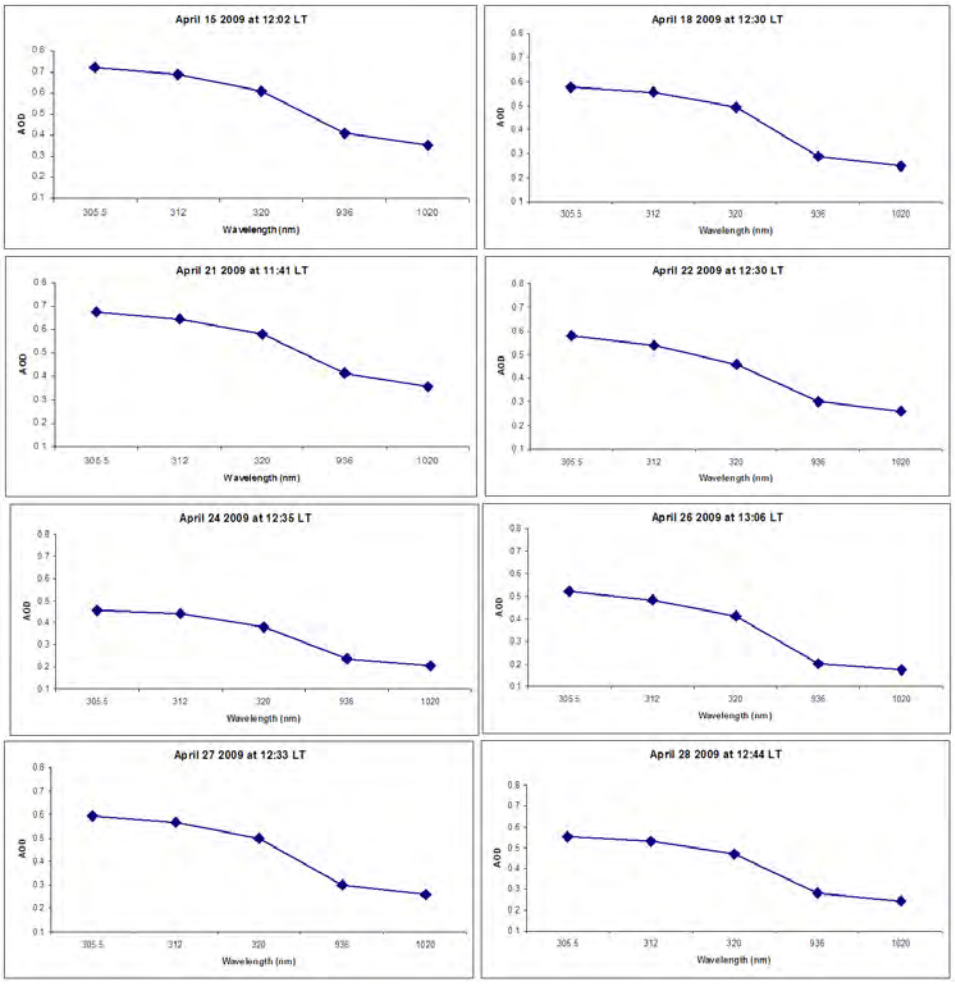
April 15 2009 at 12:02 LT
April 18 2009 at 12:30 LT
April 21 2009 at 11:41 LT
April 22 2009 at 12:30 LT
April 24 2009 at 12:35 LT
April 26 2009 at 13:06 LT
April 27 2009 at 12:33 LT
April 28 2009 at 12:44 LT
AOD
Wavelength (nm)
305.5
312
320
936
1020

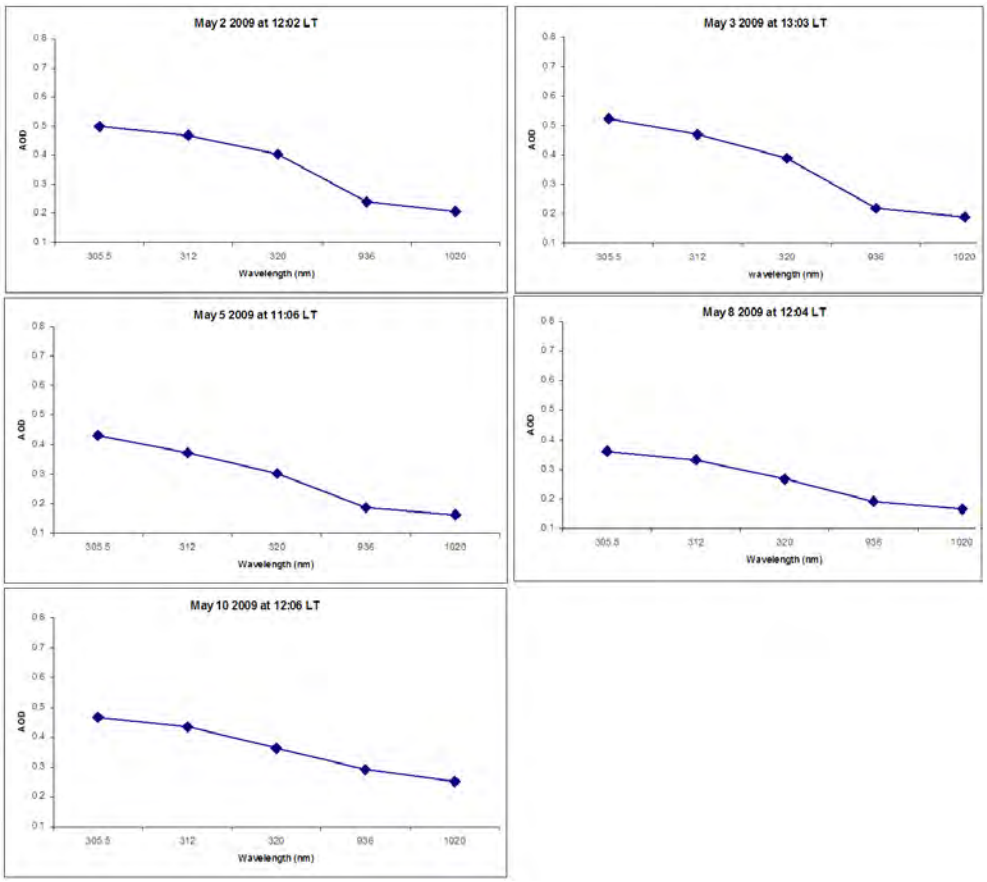

Figure 6.1: Wavelength dependance of AOD on clear sky days from March 20 to May 10, 2009 at typical time.

from the Somalia as confirmed from trajectory analysis (See Fig. 6.2).

Fig. 6.1 also reveals that AODs of April 24 and 26, 2009 are observed to be small as compared to the other days of the measurements of the month, whereas they are comparable to the AODs of most of the measurements of the other months. As evident from the back trajectory Fig. 6.2 this is attributed to the air mass of these days have different source from the air masses in April but similar source to the other months. The back trajectory also reveals that the air masses on March 20 and 29, 2009 have similar source. However, the AODs of March 20, 2009 are observed to be smaller than that of March 29, 2009. This may be attributed to the topography of the measurement site hence these air masses are injected from the north-east they may have a chance to be blocked by the mountains.

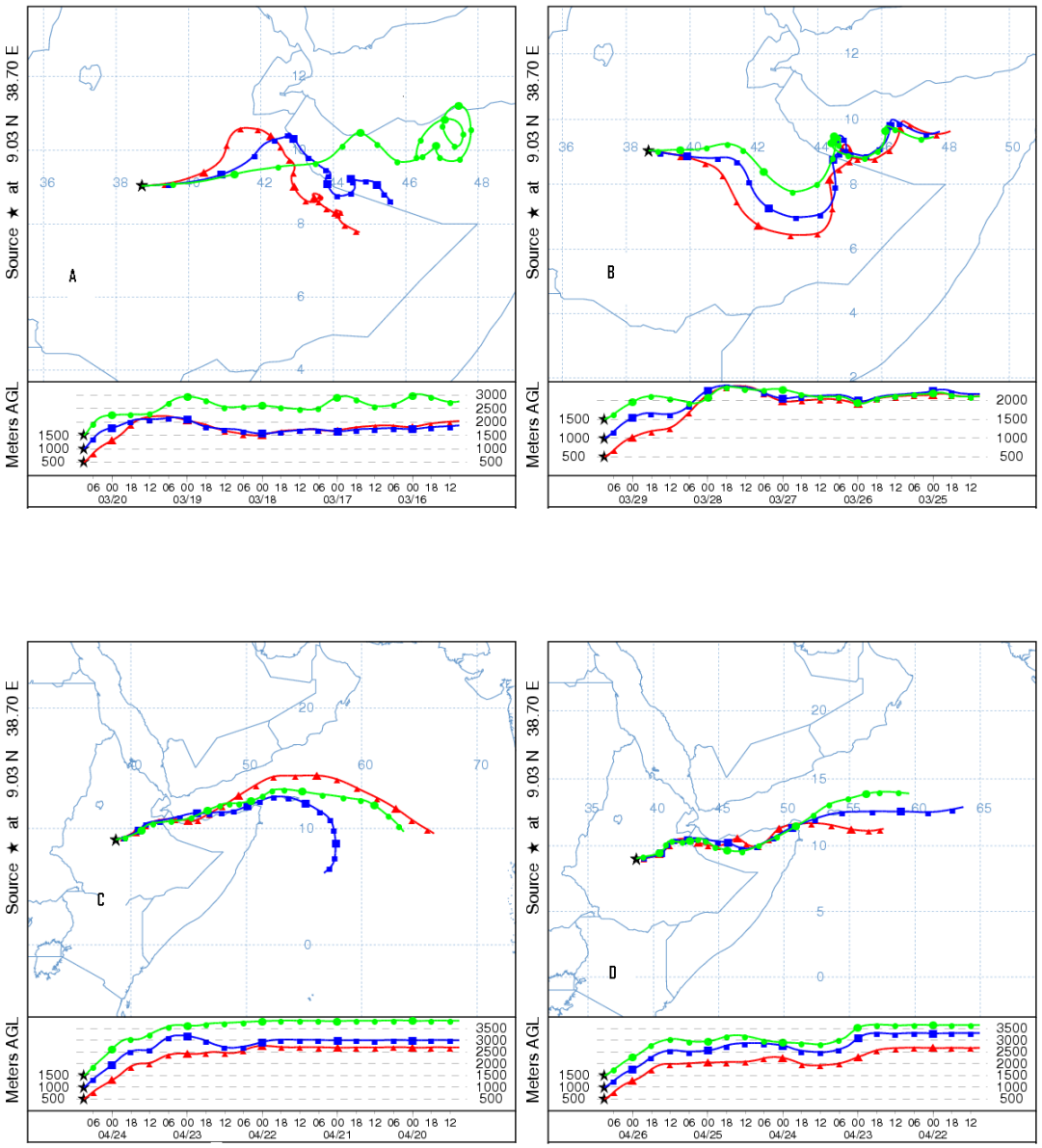

Figure 6.2: Five days backward trajectories starting from Addis Ababa (9.033N, 38.7E) at 12:00 LT on (A)March 20, 2009, (B)March 29, 2009, (C) April 24, 2009, and (D) April 26, 2009.

6.2 Day-to-day Spectral-Temporal variation in Aerosol Optical Depth

The capability of MICROTOPS-II to make high resolution measurements has been used to study the temporal variations in AOD, aerosol size distribution (ASD) and Angstrom parameters (derived from spectral AOD). Such a study is very significant to understand the variability of aerosol loading having different sizes. Fig. 6.3 depicts the spectral-temporal variation of AOD for optical channels (305.5, 312, 320, 936 and 1020 nm) on a typical clear-sky days from March 20 to May 10 2009. It is evident that the AOD values are high for smaller wavelengths and vice versa, which clearly agrees with a systematic spectral dependance according to classical Mie scattering theory. Large variability of AOD is observed for some days during our observation which decreases with increasing wavelength. This indicates that the presence of fine mode aerosols injected to the experimental area with a small mixing to the coarse mode aerosols. It is also clear that aerosol optical depth at these wavelengths exhibit a temporal pattern with high values before and after noon time and minimum at noon time (12:00-13:00 LT). It may be due to the high temperature, low relative humidity and short path length during the noon time.

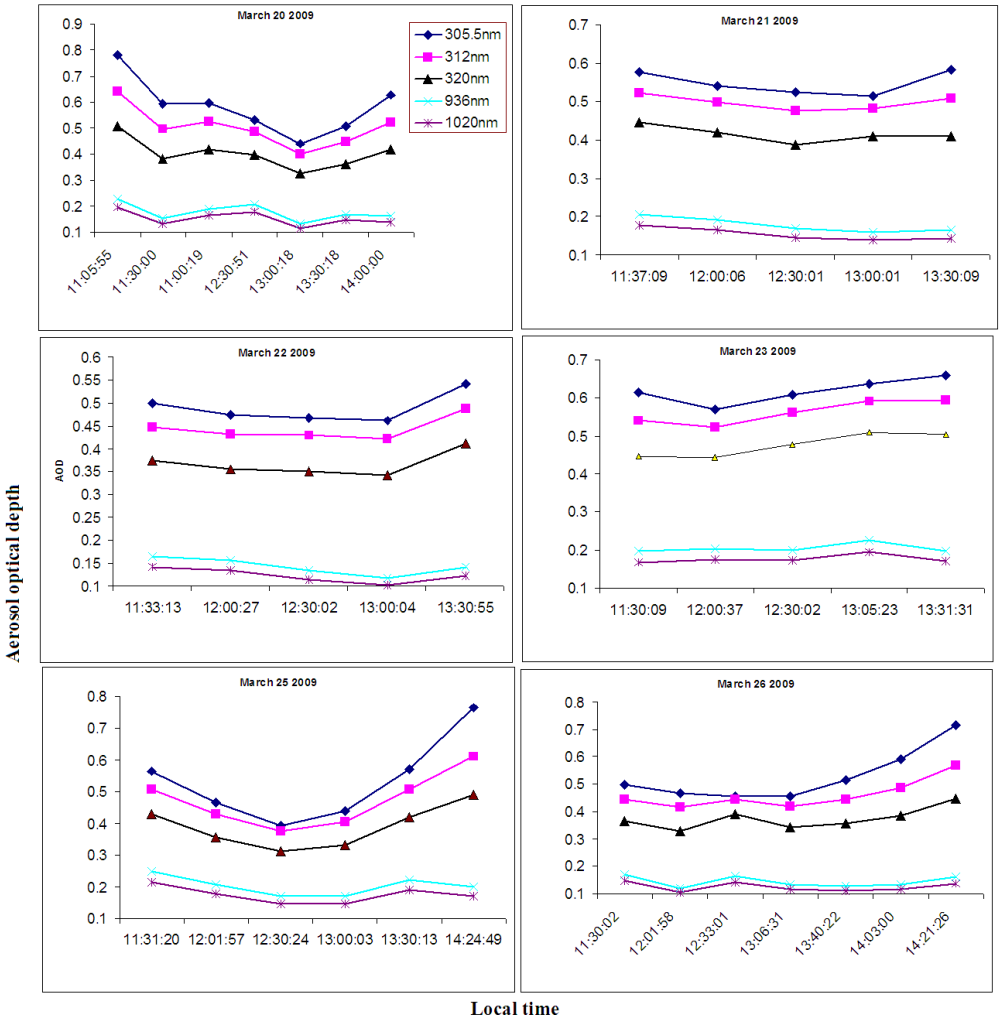
March 20 2009
305.5nm
312nm
320nm
936nm
1020nm
11:05:55
11:30:00
11:00:19
12:30:51
13:00:18
13:30:18
14:00:00
March 21 2009
11:37:09
12:00:06
12:30:01
13:00:01
13:30:09
March 22 2009
AOD
11:33:13
12:00:27
12:30:02
13:00:04
13:30:55
March 23 2009
11:30:09
12:00:37
12:30:02
13:05:23
13:31:31
March 25 2009
11:31:20
12:01:57
12:30:24
13:00:03
13:30:13
14:24:49
March 26 2009
11:30:02
12:01:58
12:33:01
13:06:31
13:40:22
14:03:00
14:21:26
Aerosol optical depth
Local time

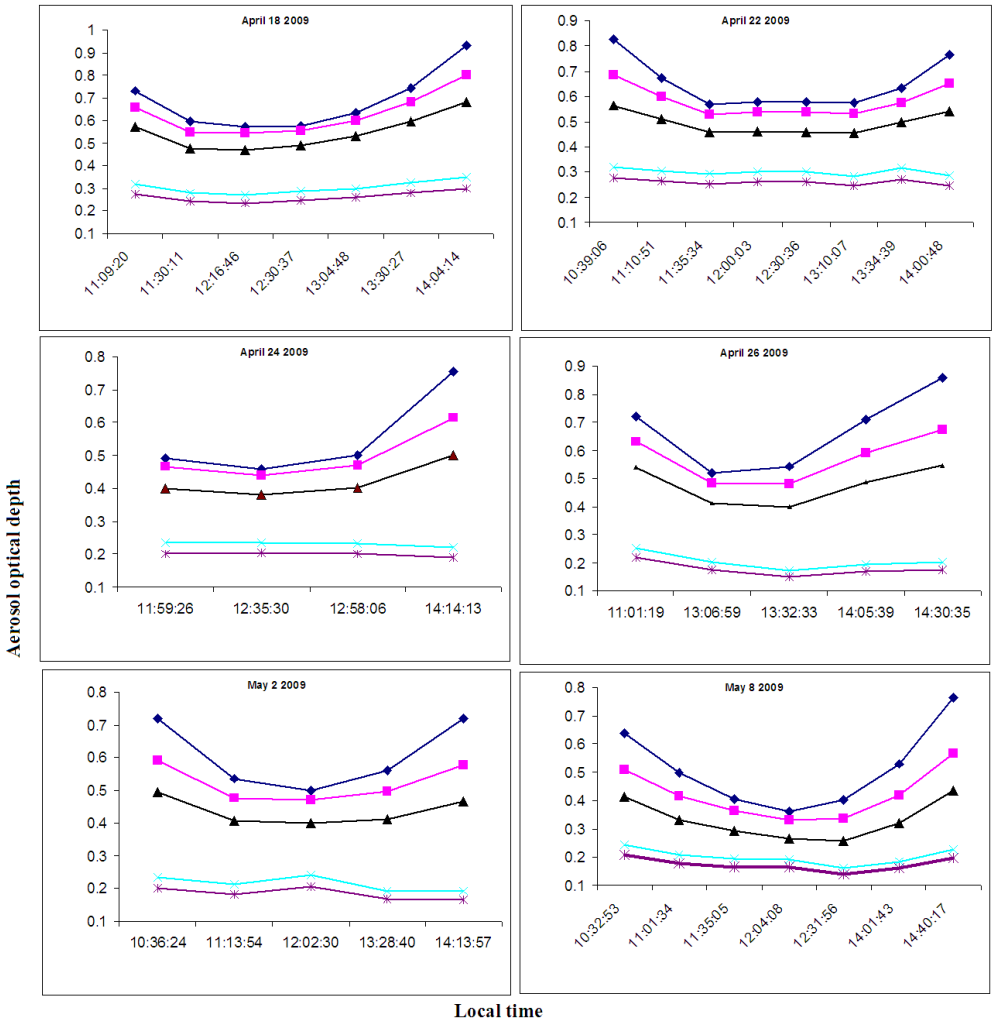

Figure 6.3: Day to day spectral-temporal dependance of AOD

6.3 Day-to-day Temporal Variation of Angstrom parameters

The Angstrom wavelength exponent α and turbidity coefficient β have been calculated at a wavelength of 320 nm and 936 nm using Eqn. (5.3.3). The values of these parameters verses time for most of the experimental days are plotted in Fig. 6.4. Our data reveals an inverse relation relationship between α and β values, i.e. the low exponent α values are associated with the high β values and vice-versa. This is in agreement with existing understanding that the higher the radius of the aerosol particle the lower the amount in the atmosphere.

The correlation coefficient between α and β is estimated and shown in Fig. 6.5. The correlation coefficient (R=-0.807) indicates a very good anti correlation between α and β. The values of α is found relatively small in all our observation times ranging from 0.993 to 0.204 with a mean value of 0.627. This indicates the presence of coarse-mode aerosol particles in the study area during the observation period.

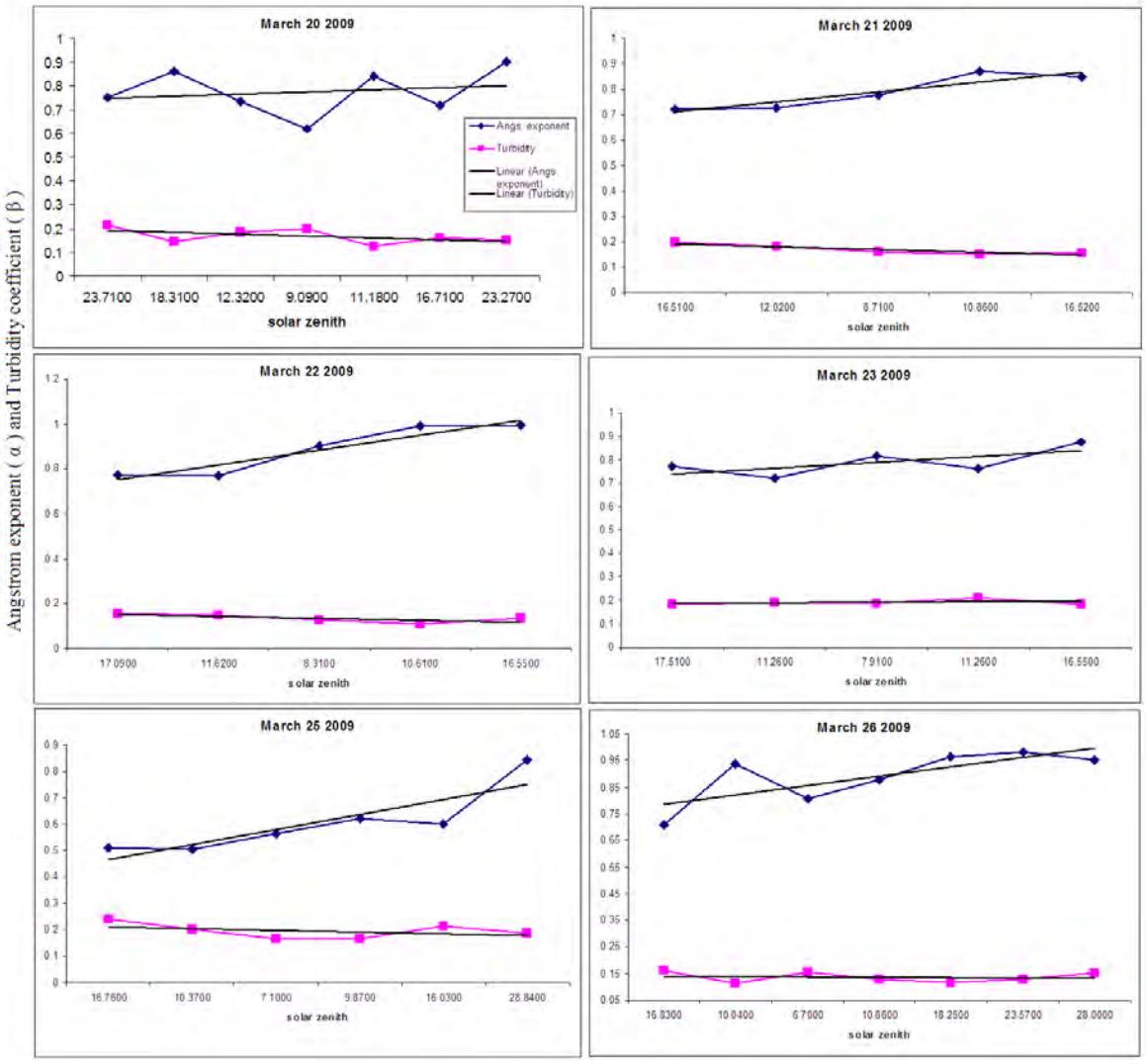
Angstrom exponent (α) and Turbidity coefficient (β)
March 20 2009
Angs. exponent
Turbidity
Linear (Angs. exponent)
Linear (Turbidity)
23.7100 18.3100 12.3200 9.0900 11.1800 16.7100 23.2700
solar zenith
March 21 2009
16.5100 12.0200 8.7100 10.8600 16.5200
solar zenith
March 22 2009
17.0900 11.6200 8.3100 10.6100 16.5500
solar zenith
March 23 2009
17.5100 11.2600 7.9100 11.2600 16.5500
solar zenith
March 25 2009
16.7600 10.3700 7.1000 9.8700 16.0300 28.8400
solar zenith
March 26 2009
16.8300 10.0400 6.7000 10.8600 18.2500 23.5700 28.0000
solar zenith

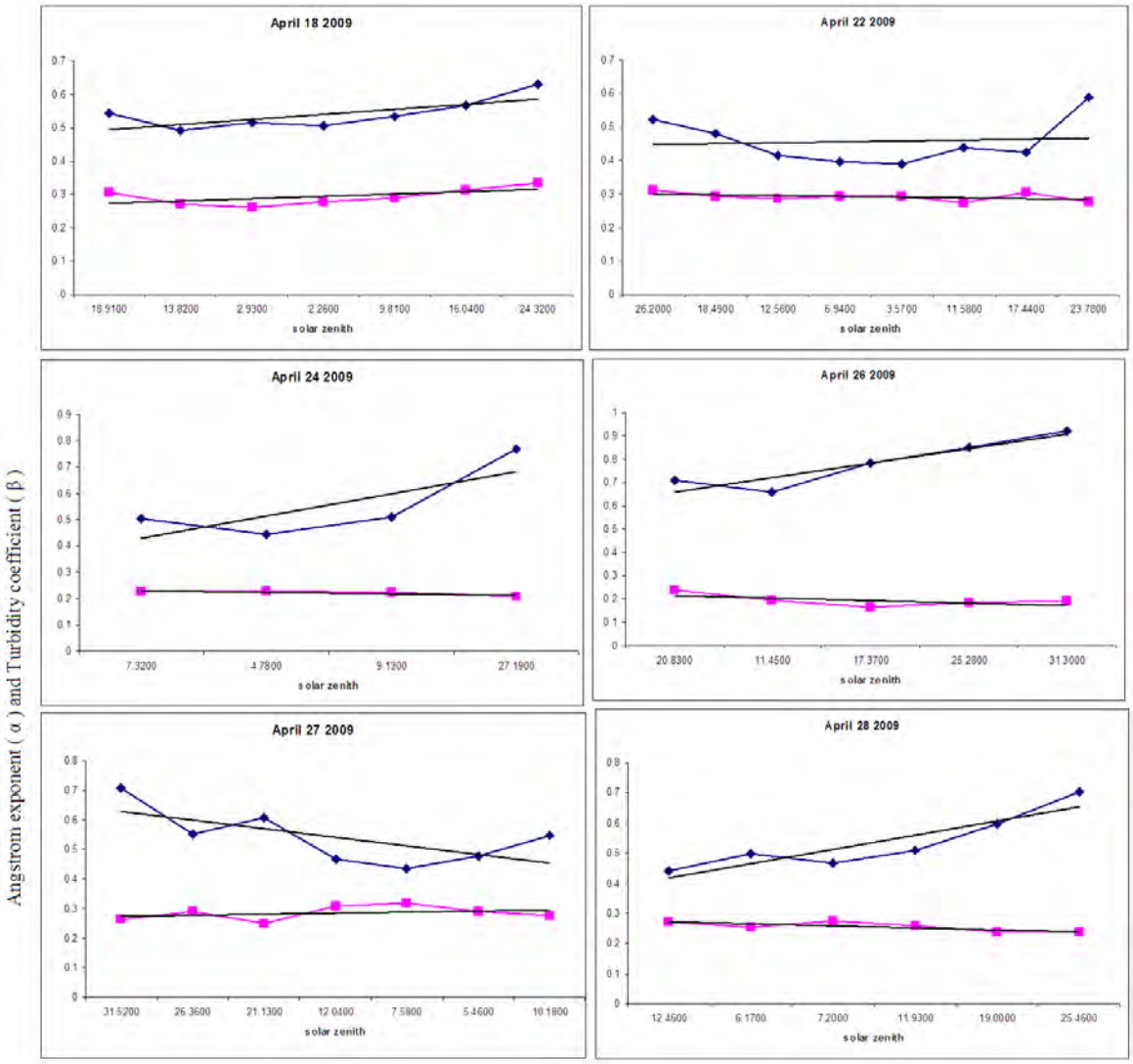
April 18 2009
18.9100
13.8200
2.9300
2.2600
9.8100
16.0400
24.3200
solar zenith
April 22 2009
26.2000
18.4900
12.5600
6.9400
3.5700
11.5800
17.4400
23.7800
solar zenith
April 24 2009
7.3200
4.7800
9.1300
27.1900
solar zenith
April 26 2009
20.8300
11.4500
17.3700
25.2800
31.3000
solar zenith
April 27 2009
31.5200
26.3600
21.1300
12.0400
7.5800
5.4600
10.1800
solar zenith
April 28 2009
12.4600
6.1700
7.2000
11.9300
19.0000
25.4600
solar zenith
Angstrom exponent (α) and Turbidity coefficient (β)

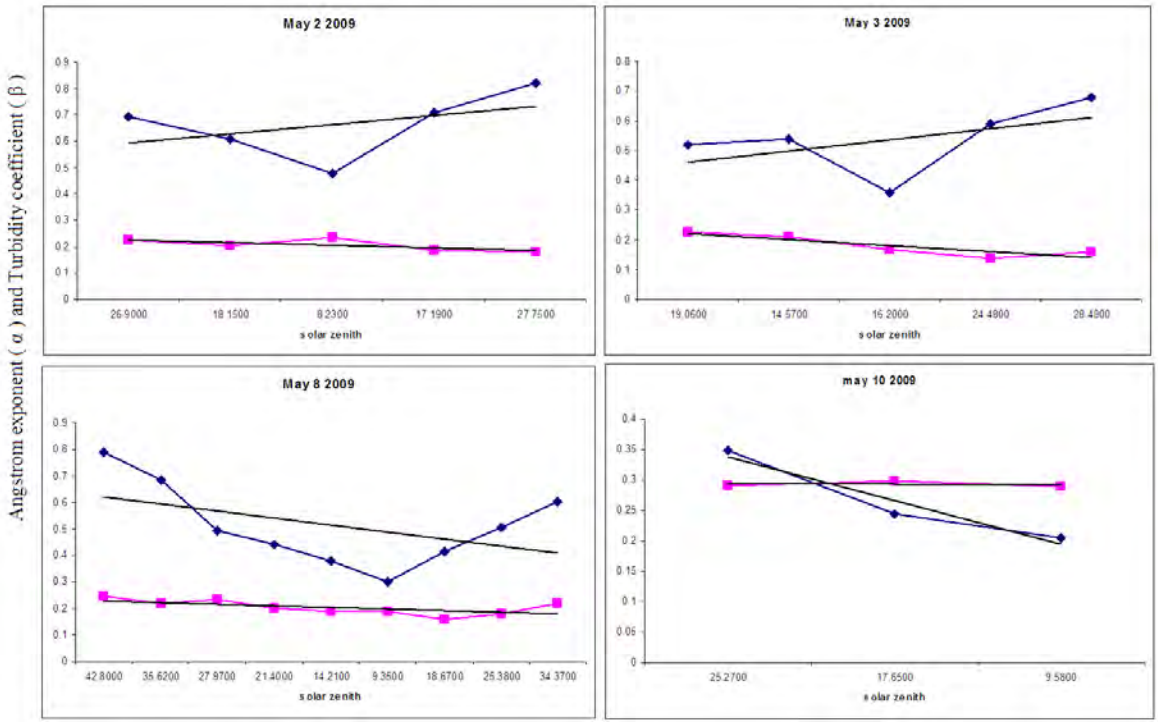

Figure 6.4: Temporal variation of angstrom exponent α and turbidity coefficient β with solar zenith angle for most of the experimental days

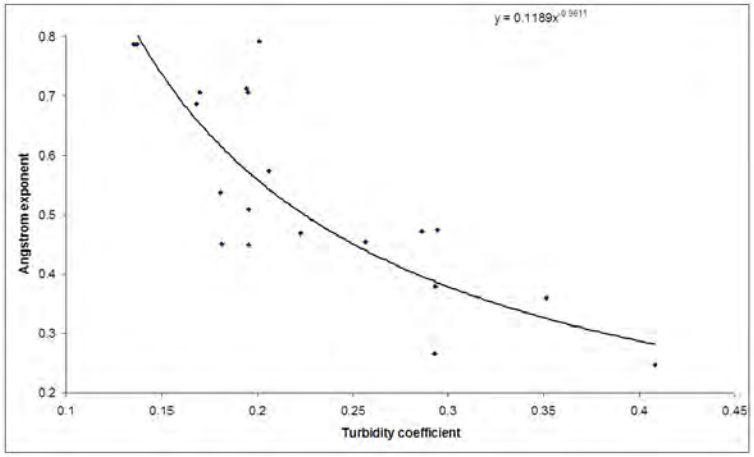

Figure 6.5: The relationship between the angstrom exponent α and turbidity coefficient β

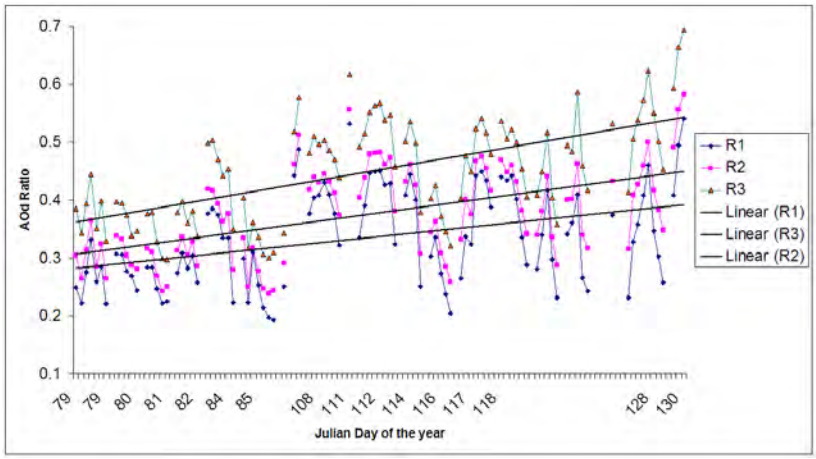

Figure 6.6: The ratio of AOD at the larger wavelength to the smaller wavelength verses time for each measurement days

The ratio of AOD measured at 1020 nm (which characterize coarse mode particles) to the other three wavelengths 305 nm, 312 nm, and 320 nm (which characterize fine mode particles) R1, R2 and R3 respectively are plotted in Fig. 6.6. This plot clearly indicates larger ratio in late April days, implying the abundance of more coarse-mode particles during these time in the study area. As it is evident from the back trajectory analysis most of the air mass injected to the experimental area are form the Somalia, middle east countries.

6.4 Day-to-day Variation of Mean Aerosol Optical Depth

Fig 6.7 shows daily variation of mean AOD at five characteristics wavelengths as 305 nm, 312 nm, 320 nm, 936 nm and 1020 nm. The last two channels represent coarse modes whereas the first three channels represent the fine mode aerosol particles. For the measurements of March and May large variability in AODs are observed which decreases with increasing wavelength. This is attributed to long range transported aerosols from higher altitudes and relatively form the same region. Whereas, in April large variability in AODs are observed at larger wavelength too. This is due to the long range transported aerosols from different sources with high mixing to the lower altitude aerosols. The highest daily mean of AODs was found to be 0.729 on March 29, and for most days in April, 2009. These remarkably higher values of AOD is attributed an increased aerosol input due to the long range transported aerosols from the Somalia and middle east countries. The AODs for the measurements of April, 2009 are observed to be relatively higher. This indicates that the presence of strong source of aerosols during these time.

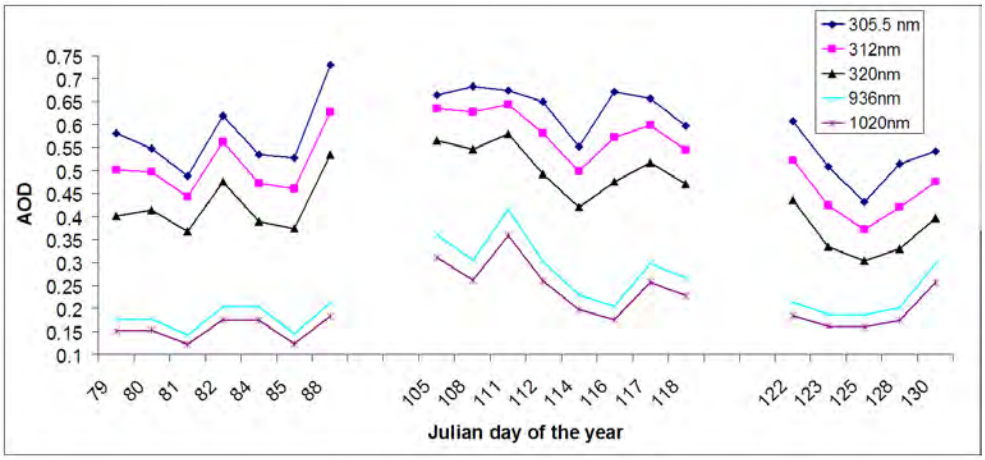

Figure 6.7: Mean AOD day-to-day variation

6.5 Day-to-day Variation of Mean Angstrom Parameters

The wavelength dependance of AOD is usually represented by the Angstrom coefficients such as Angstrom exponent α and turbidity coefficient β, which indicates size and concentration of aerosol particles, respectively. Daily variation of α and β, ranging from 0.792 to 0.247 and 0.408 to 0.135 respectively are shown in Fig. 6.8. An inverse relationship between these two parameters was observed on most of the experimental days, i.e. the low α values are associated with the high β values and vice-versa. The relatively smaller values of α is observed during the observation period which indicate the presence of coarse-mode particles on the observation site. A positive correlation between AOD and Angstrom turbidity β as clearly observed from Fig 6.7 and Fig 6.8 indicates the Angstrom turbidity can be used as a measurement of aerosol optical depth at large wavelength.

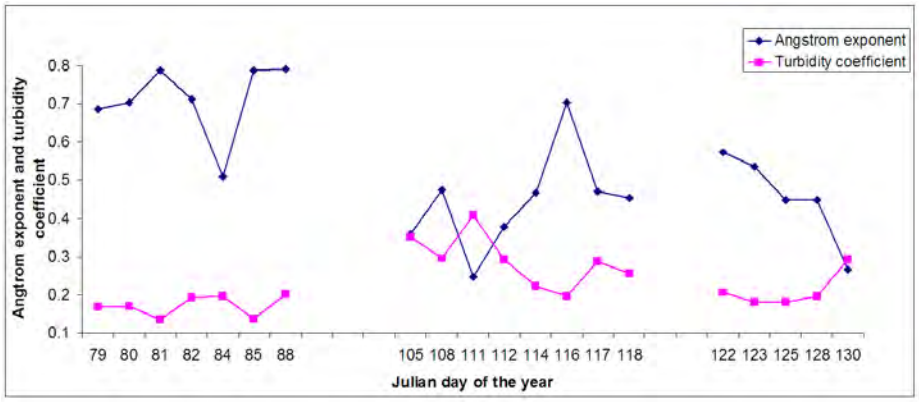

Figure 6.8: Mean day-to-day angstrom variation

6.6 Variation of Aerosol Size Distribution

We retrieved the columnar aerosol size distribution (ASD) from the spectral distributions of AOD by making use of the inversion technique suggested by Birhanu, (2007) following King (1978) formulations. The size distribution results are presented in terms of $n_c(r)$, which represent the number of particles per unit volume as a function of radius in a vertical column through the atmosphere. For consistency of presentation, all inversions were performed by assuming the complex refractive index of the aerosol particles were wavelength and size independent. We choose the complex refractive index to be m=1.43-0.008i and m= 1.53-0.008i. The later is to see the variation of ASD with the real part of the refractive index. Although these values were arbitrarily selected, there is considerable evidence that the real part of the index of refraction lies somewhere between 1.33 (pure water) and 1.54 (silicate particles).

As explained in Section (6.2) the observed temporal variation of AOD for different optical channels has been utilized to study the temporal variation of ASD. Fig.6.9

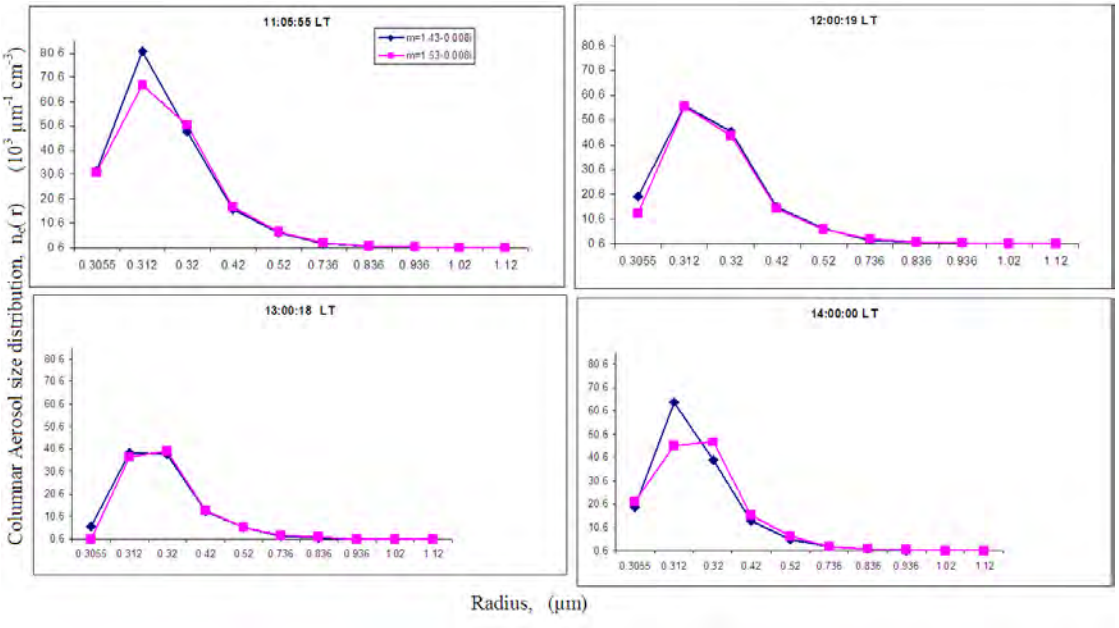

Figure 6.9: Spectral-temporal dependance of aerosol size distribution on March 20, 2009

displays hour-to hour variations in ASD observed over the station on March 20, 2009. Significant variations in ASD with time are clearly evident from Fig. 6.9. The ASD is observed to be large before noon and become minimum at noon then starts to increase in the after noon. It also reveals that large ASD variability at smaller radius which decreases with increasing radius. These relations are in good agreement with what we discussed on the temporal variation of AOD. This indicates that the spectral variation of AOD is directly depends on aerosol size distribution.

Change in the real part of the complex refractive index, which depends on the chemical nature of aerosols, produce a change in magnitude of the retrieved columnar size function $n_c(r)$ this is an evidence that the columnar concentration of aerosol in the

atmosphere depends not only on their microphysical property but also on there chemical properties.

Using the day-to-day mean AOD values we retrieve the the columnar aerosol size distribution for each days of the measurement. Results are plotted in Fig. 6.10 so as to illustrate the day-to-day mean variations of ASD. The columnar aerosol concentration observed to be large with large variability during the measurements of April, 2009 as compared to the measurements of March, 2009. Fig. 6.10 also reveals the columnar aerosol concentration on April 24 and 26, 2009 are lower and found to be in the range of the columnar aerosol concentration of March, 2009. These properties have been discussed from the measurements of AODs. This suggests that the aerosol optical properties contain information about the microphysical property of aerosols.

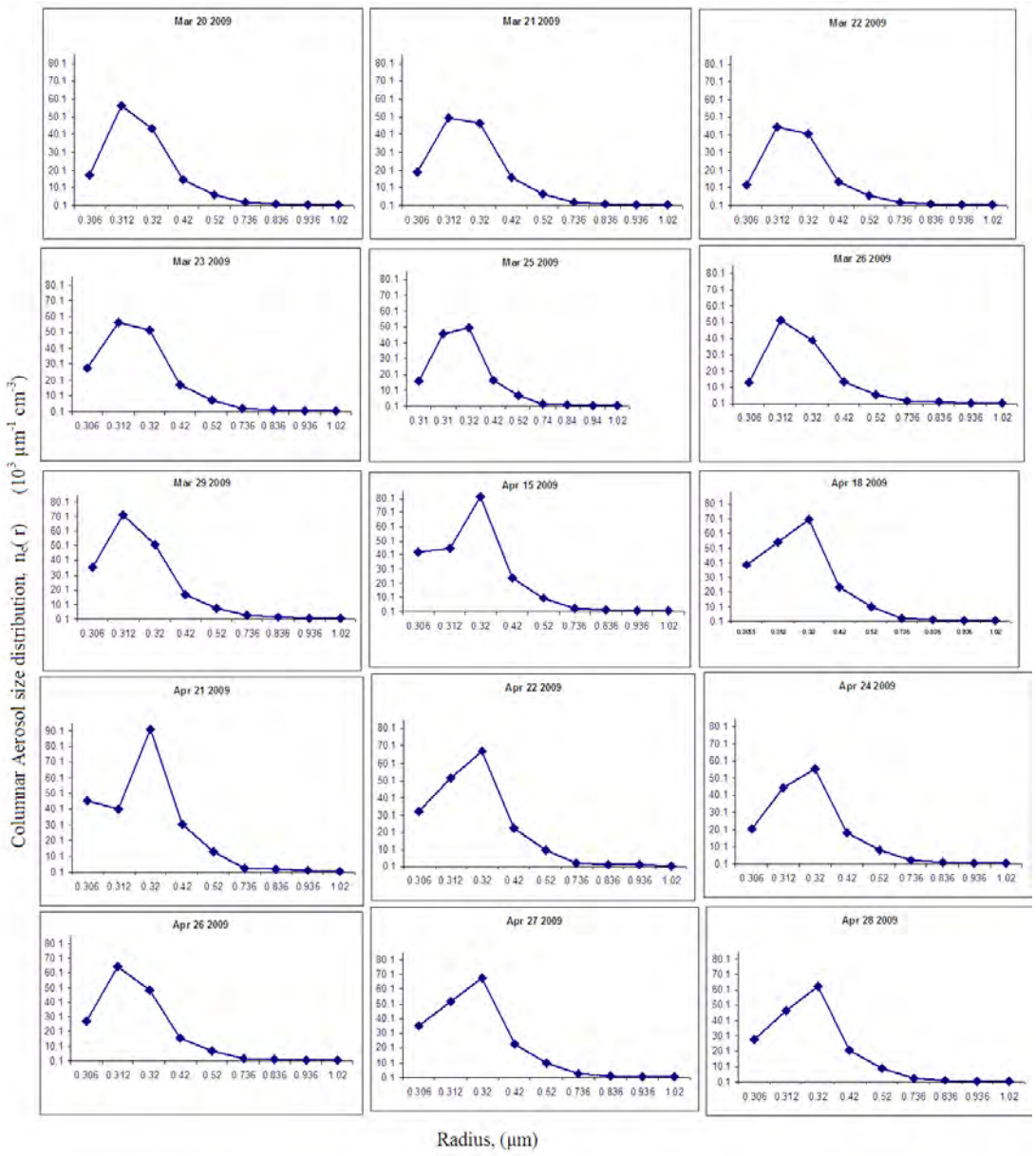

Figure 6.10: Day-to-day Mean ASD variation on March and April,2009

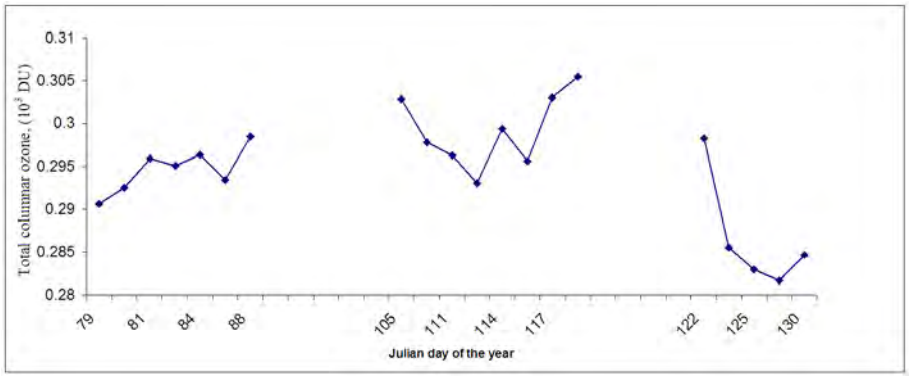

Figure 6.11: Day-to day variation of total columnar ozone

6.7 Total Columnar Ozone Measurements

MICROTOPS-II provides Total Columnar Ozone (TCO) by making use of differential absorption of irradiance at 305.5, 312 and 320 nm for ozone. High resolution measurements of columnar ozone from MICROTOPS-II have been used to examine the temporal variation of Total Columnar Ozone. Fig.6.11. portrays mean variations of ozone observed over the station during clear sky days of March 20 to May 10, 2009. Day-to-day variations in ozone concentration can be seen from Fig. 6.11 with significant fluctuations, The mean column ozone over the station was observed within the range from 281.6-305.4 DU with a mean value of 294.5 DU during the study period. TOMS satellite data shows the ozone variation for the experimental period within the range of 259 - 267 DU. Our results show 9 *to* 12% progress from TOMS satellite data.

6.8 Association between columnar aerosol optical depth and precipitable water content

In addition to the ozone and aerosol measurements, MICROTOPS-II provides precipitable water content (PWC) by making use of differential absorption of irradiance at 940 and 1020 nm for retrieving the precipitable water content. The mean variation of PWC over the station shows maximum frequency of occurrence of mean PWC ranging between 0.422 and 1.3 cm. Fig.6.12 shows daily variations in columnar AOD at 1020 nm, PWC and RH over the experimental station during March 20 - May 10, 2009. The mean column values of AOD and PWC were observed about 0.209 ($\pm$0.0625), and 0.756 ($\pm$0.186) cm respectively over the study area. In March and May significant positive correlation between AOD and PWC was observed, suggesting the growth of aerosol particles with atmospheric PWC, which are hygroscopic in nature. Whereas, in April, insignificant correlation was observed between AOD and PWC which indicates that the presence of non-hygroscopic aerosols. In order to study the above aspect, 5-days air mass back-trajectories obtained from the NOAA HYSPLIT model at three different height levels of 500, 1000 and 1500 m (AGL) have been plotted in Fig. 6.13 (A) for March 23 (B) for March 23 (C) for April 21 and (D) for April 22, 2009. It is evident from the figure that the air mass in March and May are injected to the experimental site from the Indian ocean, which is the main source for marine aerosols, so hygroscopic aerosols dominates the atmosphere. Whereas the aerosols injected to the experimental site in April are from the middle east countries with a small mixing to the red sea for most of the days, so none hygroscopic aerosols dominate the atmosphere. The trajectory also reveals that in April the air masses are lifted up from the surface of the Middle East Countries.

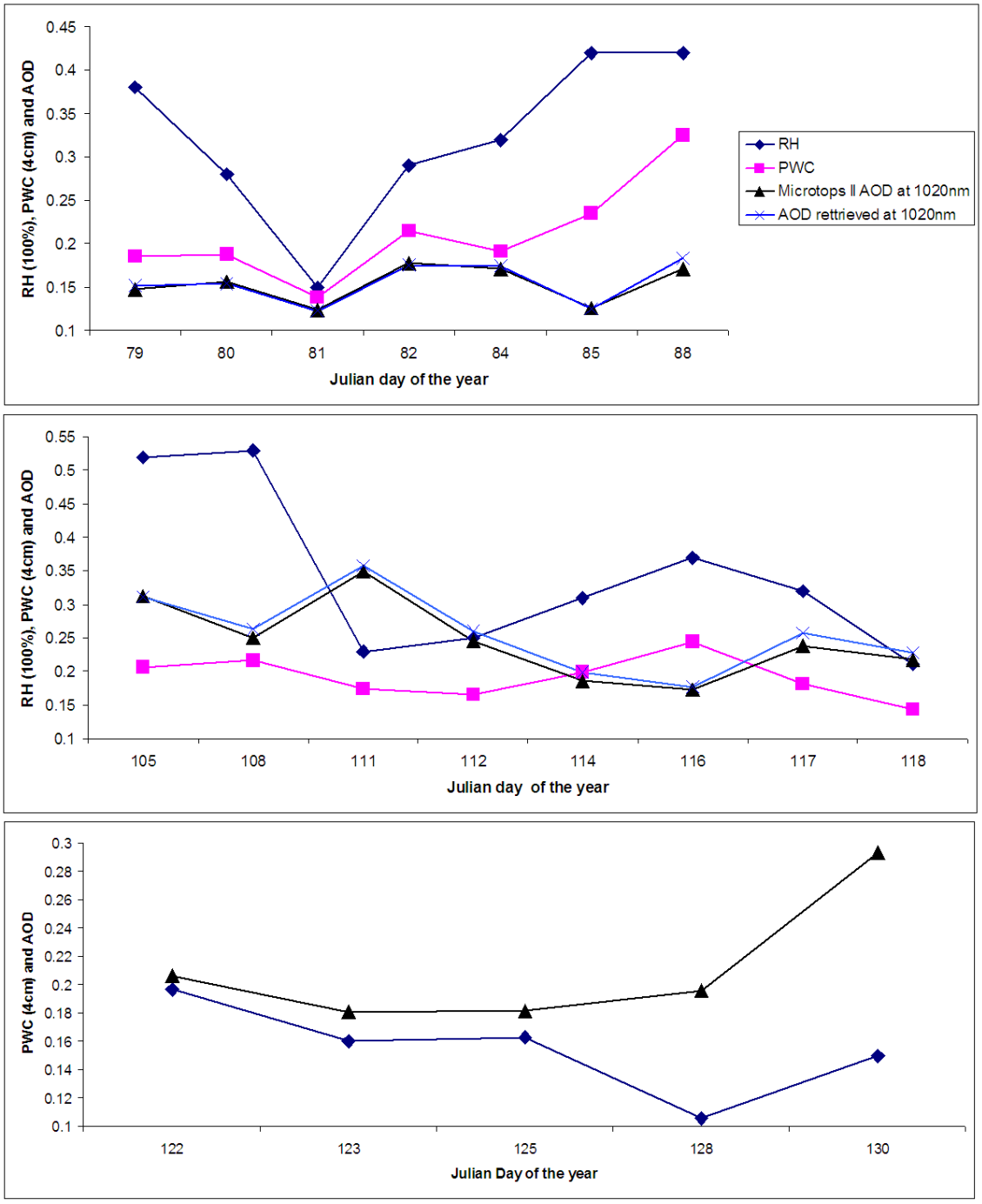

Figure 6.12: Association between relative Humidity (RH), precipitable water (PWC) and Aerosol Optical Depth (AOD) at 1020nm

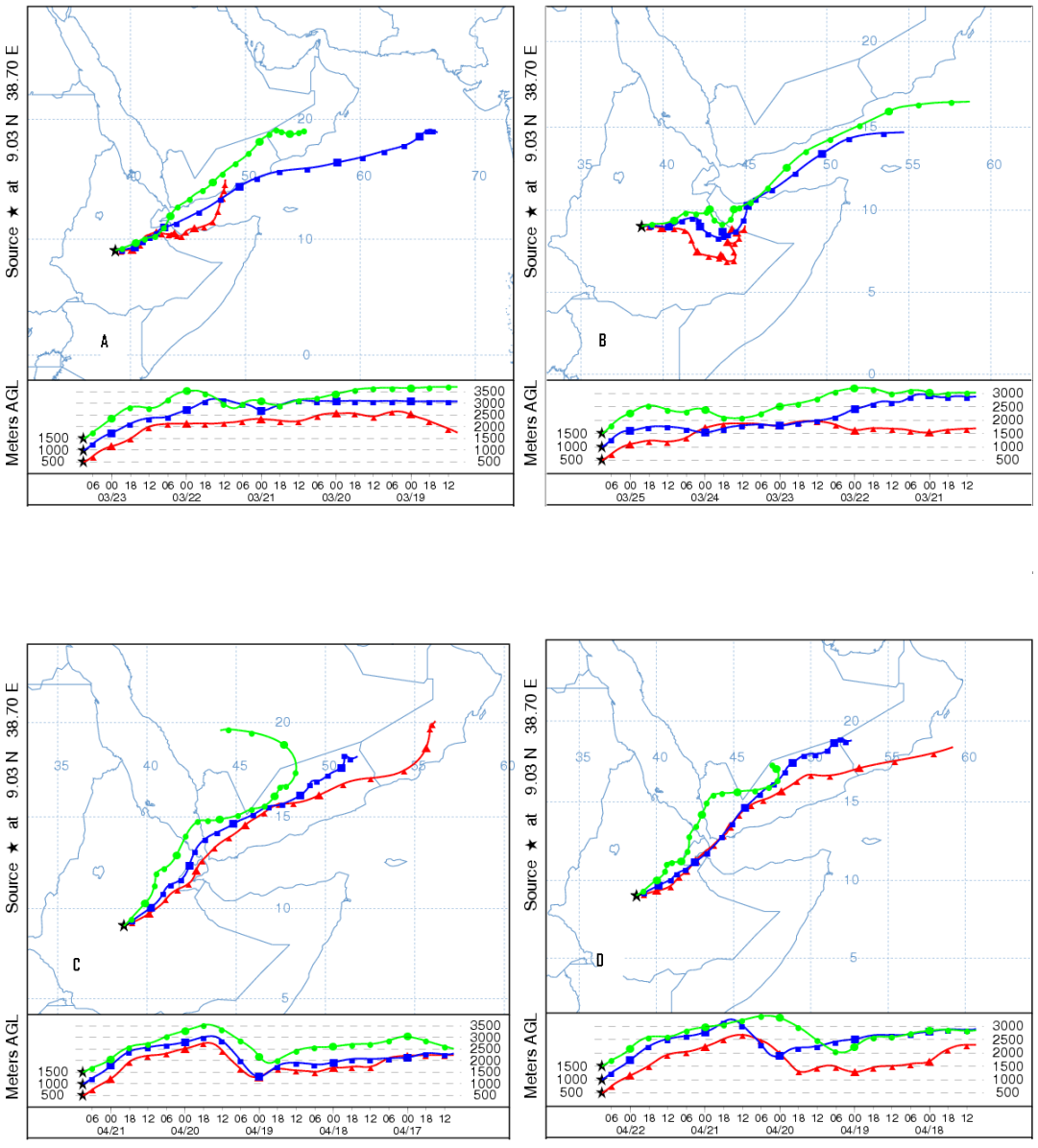

Figure 6.13: Five days backward trajectories ending at 12:00 LT at Addis Ababa on (A)March 23, 2009, (B)March 25, 2009, (C) April 21, 2009, and (D) April 22, 2009.

Chapter 7

Conclusions

In this thesis we study the aerosol microphysical and optical properties, total columnar ozone and precipitable water content over Addis Abeba at (9.033N and 38.7E)at an altitude of 2445m a.m.s.l. by measuring the direct solar irradiance using 5-channel Microtops II sunphotometer (Solar Light Co., USA) for clear sky days from March 20, to May 10, 2009.

The Microtops II gives the total columnar ozone in Dobson unit and the amount of precipitable water content in cm from differential irradiance measurements at 305.5nm, 312nm and 320nm for ozone measurements and 936nm and 1020nm for precipitable water content measurements. We used the measured irradiance at these five different wavelength in the range between 305.5 - 1020nm as an input to calculate the aerosol optical depth at these 5-channels using the Beer-Budger law. Following the inversion techniques suggested by King et al. (1978) we retrieved the aerosol size distribution. We also calculated the Å ngstrom exponent and turbidity coefficients using the aerosol optical depth at 320nm and 936nm wavelengths. To explain the extreme values in AOD and the relation between AOD and precipitable water content

of the atmosphere we use a 5-day backward trajectory starting from the experimental site.

The results of the study indicate the aerosol optical depth shows a spectral variation which gradually decreases with increasing wavelength as expected from the classical Mie theory. Temporal variation of aerosol optical depth and aerosol size distribution are minimums at the noon time(12:00-13:00 LT). An inverse relation between the Ångstrom exponent and the turbidity coefficients with a good anticorrelation (R=-0.807). A small value of Ångstrom exponent range from (0.204) to (0.993) with a mean value (0.627) during the measurement period indicates the presence of coarse mode particles on the atmosphere.

A change in complex refractive indices changes the shape and magnitude of retrieved aerosol size distribution. Since the complex refractive index are dependent on chemical composition of the particles. The microphysical properties of aerosols depends on their chemical composition. A significant positive correlation between aerosol optical depth and precipitable water content during March and May indicates the air masses load on the atmosphere are marine aerosols from the Indian ocean which are hygroscopic in nature. Insignificant correlation between aerosol optical depth and precipitable water content during April, 2009 indicates the air mass load on the atmosphere during this month is dust aerosols from Middle East counties which are non hygroscopic in nature.

Bibliography

[1] Alexander, Dr. and Kokhanovsky,A. (2008). *Aerosol Optics Light Absorption and Scattering by Particles in the Atmosphere*, Springer and Praxis Publishing, Germany.

[2] Birhanu Asmerom (2007). *modeling interaction of radiation with aerosol using Mie scattering formulation and retrival of aerosol size parameters*, MSc. Thesis, Addis Ababa University.

[3] Detlev, M. (1999). *Atmospheric Environmental research*, critical decisions betwen thechnological progress and preservation of nature, springer-Verlag, printed in Germeny.

[4] Devara, P.C.S., Pandithurai, G., Raj, P.E. and Sharma, S. (1996). *Investigations of Aerosol Optical Depth Variations Using Spectroradiometer at an Urban Station, Pune, India.* J. Aerosol Sci. vol. 27, pp. 621632.

[5] Dubovik,O., Holben,B., Eck.F.T., et.,al.(2001). *Variability of Absorption and Optical proerties of key Aerosol types observed in world wide locations*, Jouranal of the atmospheric science.

[6] Dubovik, O. V., Lapyonok, T. V. and Oshchepkov, S. L. (1995). *Improved technique for data inversion: Optical sizing of multicomponent aerosols*, Appl. Opt., Vol. 34, pp. 8422-8436.

[7] Eyre,J. R. (2001). *Inversion methods for satellite sounding data*, Meteorological Training Course Lecture Series, 9 January 2001.

[8] Fleagle, R. G. and Businger, J. A.(1980). *An Introduction to Atmospheric Physics*, 2^{nd} edition, International Geophysics Series, vol. 25, Acadamic Press, New York.

[9] Hanel, G. (1972). *Computation of the Extinction of Visible Radiation by Atmospheric Aerosol Particles as a Function of the Relative Humidity, Based Upon Measured Properties*, Journal of Aerosol Science . vol. 3, pp. 377386.

[10] Herman, B. M., Browning, S. R. and Reagan, J. A. (1971). *Determination of aerosol size distributions from lidar measurements*, Journal of Atmospheric science, vol. 28, pp. 763-771.

[11] Godish, T. (2004). *Air quality*, 4^{th}. Lewiss publisher, printed in the united states of America.

[12] King et al. (Nov 1978). *Aerosol Size Distributions Obtained by Inversion of Spectral Optical Depth Measurements*, Journal of Atmospheric science, Vol. 35, No. 11, pp. 2153-2167.

[13] Kondrat'ev, K. Ya.(1969). *Radiation Characteristics of the Atmosphere and the Earth's Surface*, Translated from Russian, Amerind publishing, New Delhi.

[14] Kuzmanoski, M., Box, M. A., Box, G. P., Schmid, B., Wang, J., Russell, P. B., Jonsson, H. H. and Seinfeld, J. H. (2007) *Aerosol Properties Computed from Aircraft-Based Observations during the ACE-Asia Campaign: Aerosol Size Distributions Retrieved from Optical Thickness Measurements*, Aerosol Science and Technology, vol. 41, pp. 202216.

[15] Latha, K. M., Badrinath, K.V. (2004). *Studies on atmospheric turbidity over a tropical urban environment*, Atmospheric Science letters, Vol. 5, pp. 134-139.

[16] Liou, K. N. (2002). *An Introduction to Atmospheric Radiation*,2^{nd} edition, International Geophysics Series, vol. 84, Acadamic Press, New York,

[17] Liu, L., Lacis, A. A. and B. E. Carlson, (2005). *Improving GCM Aerosol Climatology using Satellite and Ground-Based Measurements*, Fifteenth ARM Science Team Meeting Proceedings, Daytona Beach, Florida, March 14-18.

[18] Meloni, D. (2000). *Optical properties and radiative effects of tropospheric aerosols and ozone in central Meditranian*, PhD. Thesis, UNIVERSIT DEGLI STUDI DI ROMA.

[19] Mishehenko,Michael.I., Travis,Lary,D., and Lacis, Andrew,A.(2005). *Scattering and Absorption, and Emission of light by small particles*, Cambridge university press, New york.

[20] Molina, L. T. and Molina, M. J. (1986) *Absorption cross section of ozone in the 185 to 350 nm wavelength range*, J. Geophys. Res., vol. 91, pp. 14501-508.

[21] Morys, M., Hagerup,F. M., Anderson, S., Baker, S. E., and Walkup, J. T. (2001) *Design, Calibration, and Performance of Microtops II Handheld Ozone Monitor and Sunphotomerer*, Journal of Geophysics Resserch . vol. 106, pp. 14573-14582.

[22] Osterwald, C. R. and Emery, K. A. (Sep 2000). *Spectroradiometric Sun Photometry*, Journal of Atmospheric and Oceanic Technology, vol. 17, Issue 9, pp. 11711188.

[23] Raj, P.E., Devara, P.C.S., Maheshkumar, R.S., Pandithurai, G., Dani, K.K., Saha, S.K., Sonbawne, S.M. and Tiwari, Y.K. (2004). *Results of Sun Photometer-Derived Precipitable Water Content Over a Tropical Indian station*, J. Applied . Meteorology., 43: 1452-1459.

[24] Ranjan et al.,(2007). *Spectral Variation of Total Column Aerosol Optical Depth over Rajkot: A Tropical Semi-arid Indian Station*, Aerosol and Air Quality Research, Vol. 7, No. 1, pp. 33-45.

[25] Seinfeld, J.H., and Pandis, S.N.(1997). *Atmospheric chemistry and physics: from air pollution to climate change*, NewYork: Wiley.

[26] Scales,J. A., Smith, M. L. and S. Treitel, (2001).*Introductory Geophysical Inverse Theory*, Samizdat Press.

[27] Yamamoto, G., and Tanaka, M. (1969). *Determination of aerosol size distribution from spectral attenuation measurements*, Appl. Opt., Vol. 8, pp. 447-453.

[28] Voutilainen,A., Kolehmainen, V. and Kaipio, J. P. (Sep 2000). *Statistical inversion of aerosol size measurement data*, University of Kuopio, Department of Applied Physics, report No. 3, finland.